Doctoral Theses at NTNU, 2006:176

Doctoral Thesis

Shukun Chen

Rheological Properties of Water in Oil Emulsions and Particulate Suspensions

NTNU
Norwegian University of
Science and Technology
Thesis for the degree of
doctor philosophiae
Faculty of Natural Sciences and Technology
Department of Chemical Engineering

NTNU
Innovation and Creativity

Preface

This thesis is submitted in partial fulfillment of the requirements for the degree of Philosophiae Doctor at the Norwegian University of Science and Technology. The work has been performed at the Ugelstad Laboratory at the Department of Chemical Engineering.

I received my master degree from the Harbin Institute of Technology, in China in July 1996, and later the same year, I joined the China University of Petroleum as an assistant professor and later a lecturer. My main interest areas during this stay included colloid chemistry, oilfield chemistry and crude oil transportation. My teaching was centred on petrochemical technology. In 2003, I was accepted as a Ph. D. student in Professor Johan Sjöblom's research group at the Department of Chemical Engineering, at the Norwegian University of Science and Technology, in Norway.

The thesis consists of five papers or manuscripts. The Ph.D. work is a part of the Joint Industrial Program (JIP1) ''Particle-Stabilized Emulsions/Heavy Crude Oils'', financed by JIP1 consortium (ABB, AkerKvaerner, BP, Champion Technologies, Chevron, ENI, Hydro, Petrobras, Shell, Statoil, TOTAL and Vetco).

Acknowledgments

First, I would like to express my sincere gratitude to my supervisor, Prof. Johan Sjöblom, for accepting me into the Ugelstad Laboratory, for excellent supervision and for his efforts to establish a well-equipped lab. His enthusiasm and research attitude have been a model to follow in my research work.

I am extremely grateful to my co-supervisor, Prof. Gisle Øye, for showing me the right direction and pushing me forwards. His inspiring discussion and valuable comments on my manuscripts are gratefully acknowledged.

Dr. Magne Kawai Knag is especially acknowledged for his remarkable help in the beginning of my work in Ugelstad Lab.

I really appreciate all the JIP1 colleagues in the Ugelstad Lab., for friendly cooperation. In particular, I would like to thank Pål and Andreas for their useful discussion and great ideas.

I would like to thank Dr. Sébastien Simon for proof reading and offering me many detailed comments.

Thanks to all past and present members of the Ugelstad Lab. for their contributions to the friendly and professional environment. And special thanks to Maria, Hung-Hsun and Øystein.

Financial support from JIP1 consortium (ABB, Aker Kværner, British Petroleum, Champion Technologies, Chevron, ENI, Hydro, Mærsk, Petrobras, Shell, Statoil, Total, and Vetco) is gratefully acknowledged.

My parents and parents-in law deserve big thanks for their great support and constant encouragement.

Finally, I am sincerely grateful to my wife, Aiping, for her support and care. Our son, Zhilin, deserves special thanks for bringing us tons of happiness.

Abstract

This thesis aims at a better understanding of the rheological properties of the important colloids in oil industry, i.e. suspensions, emulsions and waxes.

The rheology of suspension system is a complex field influenced by a large range of variables. In this work, we mainly focused on the rheological properties of suspensions as a function of volume fraction of particles, particle size, surface properties, shear rate, and the nature of continuous mediums. The investigated suspensions behaved as Newtonian fluids at dilute concentration, whereas, shear thinning properties were observed at high volume fractions. The shear thinning effect increased with decreasing particle size. Ionic strength and pH are both factors affect particle interactions and consequently the rheological properties of suspensions: large and strong aggregates were formed at the isoelectric point, due to the strong attraction between particles at this point. The larger aggregates results in higher viscosity, yield stress, storage moduli and shear thinning effects. The relative viscosity of all the suspensions can be reasonably well fitted with the Krieger and Dougherty model.

Wax precipitation and deposition is a recurring challenge in transportation of crude oil. To better understand and explain these phenomena, the crystal growth of two model waxes was determined as a function of concentration, cooling rate and cooling conditions (static or dynamic). The flow and viscoelastic behaviours were investigated around the wax precipitation temperature, and the yield stress was determined after both dynamic and static cooling. Interpretation of the results was carried out in view of crystal growth and microstructure of the wax crystals.

Rheological properties of wax containing water-in-oil emulsions stabilized by asphathenes were also studied. Temperature scans of viscosity, flow measurements and yield stress measurements were carried out on these systems. The effects of water cut, amount of asphaltenes and amount of waxes were investigated. Wax content and water cut have the most pronounced effect upon the viscosity and yield stress of the systems.

List of Papers

Paper 1
Rheological Properties of Aqueous Silica Particle Suspensions.
Shukun Chen; Gisle Øye; Johan Sjöblom.
J. Dispersion Sci. Technol., (2005), 26(4), 495-501.

Paper 2
Rheological Properties of Silica Particle Suspensions in Mineral Oil.
Shukun Chen; Gisle Øye; Johan Sjöblom.
J. Dispersion Sci. Technol., (2005), 26(6), 791-798.

Paper 3
Effect of ph and Salt on Rheological Properties of Aerosil Suspensions.
Shukun Chen; Gisle Øye; Johan Sjöblom.
J. Dispersion Sci. Technol., (2007), 28(5), In press.

Paper 4
Rheological Properties of Model and Crude Oil Systems when Wax Precipitate under Quiescent and Flowing Conditions.
Shukun Chen; Gisle Øye; Johan Sjöblom.
J. Dispersion Sci. Technol., (2007), 28(7), Accepted.

Paper 5
Rheological Properties of Wax Containing Water-in-Oil Emulsion.
Shukun Chen; Gisle Øye; Johan Sjöblom, In preparation.

Additional Publications

Effects of different heavy crude oil fractions on the stability of oil-in-water emulsions - the film properties of heavy crude functional components and water system.
Yaowu Chen; Weiyu Fan; Yuanming Song; Guozhi Nan; Shuiping Li; Shukun Chen. *Petroleum Sci.* (2005), 1(2), 93-96.

Determination of acid value of crude oils by potentiometry
Xingyu Liu; Weiyu Fan; Shukun Chen; Guozhi Nan; Menglong Yang.
J. Fine Petrochemical Engineering (2004), (5), 54-57.

Conference

Characterization and Rheological Properties of Waxy oils. (Oral presentation by S. Chen)
Shukun Chen; Gisle Øye; Johan Sjöblom.
The 15th Nordic Rheology Conference, Stockholm, 2006.

Contents

1 Introduction

The oil and gas industry is faced with problems associated with transporting multiphase fluids through long distance pipelines for 100 years. Today's developments in deepwater is placing an even greater emphasis on assuring flow in challenging environments. The low temperatures and high pressures encountered in deepwater facilities and flowlines can indeed lead to the formation of hydrates, wax deposition and asphaltene precipitation that can partially or totally block production lines [1-5]. Such blockages are costly because they cause production to decrease or halt and lead to expensive remedial operations [3]. Heavy crude oils and emulsions are also relentless problems within the petroleum industry as they give rise to a variety of costly problems in terms of production loss, transport difficulties and chemical expenses.

The understanding of rheological properties of these above-mentioned systems is of great technical importance in transportation and separation of crude oils. Indeed, the knowledge of rheological parameters, such as viscosity, yield stress and so on, of crude oil/water mixtures are vital in multiphase simulation, pipeline design and fluid control, and even separator design [6]. Therefore accurate fluid characterization and prediction are of great significance in crude oil processing.

The purpose of this thesis has been to investigate the rheological behaviors of suspensions and emulsions at various conditions and reveal the connection between rheolgical responses and the microstructures and chemical nature of fluids. A range of modeling work has been done to describe and predict rheolgical properties including viscosity, yield stress and so on. The flow and viscoelastic behaviours of model waxy oils and waxy crude oils have also been studied as a function of wax composition, cooling rate and cooling conditions (static or dynamic).

2 Suspension

2.1 Introduction

A suspension is defined as a colloidal dispersion in which finely-divided solid particles are dispersed in a continuous liquid phase [7]. Suspensions are of great practical interest in both the industry and everyday life, typical applications are found in coatings and paints, printing inks, ceramics, food, pharmaceutical and household products. Suspensions are also widespread and very frequently encountered in petroleum industry, as viewed in the examples below [8]:

--well drilling mud and cementing slurries;
--reservoir particles (e.g. clay, sand, CaCO3) present in oil recovery;
--solid wax suspensions in crude oil below Wax Appearance Temperature (WAT);
--asphaltene aggregations in crude oils.

The stability of suspensions is important in many technical applications, for example in paints and coatings, ceramics, well drilling slurries and crude oil processing [9-12]. Suspensions are not thermodynamically stable and particles trend to agglomerate. The stability of colloidal particles in liquids is determined by a balance between attractive and repulsive forces. The particle interactions in colloidal systems will be discussed in the following sections. We will emphasize on silica particles in aqueous suspensions due to the importance in this thesis, since the theory for colloid stability provides the basic elements in understanding the rheological behaviour of concentrated dispersions.

2.2 Particle interaction

2.2.1 Electrostatic repulsion

Repulsive forces arise from electrostatic interactions, steric interactions or combinations of these. Generally, electrostatic interactions are significant only in aqueous dispersions, while steric interactions are effective in non-aqueous systems as well [13-16].

Origin of surface charge

Solid particles normally acquire charges when suspended in aqueous solutions. This can occur either by ion adsorption from the medium and/or differential loss of ions from the solid

crystal lattice [17]. In the case of silica particles, they generally possess a high surface potential which is due to the high density of active silanol groups (around 1.8 per nm^2) on particle surface [18]. Indeed when dispersed in aqueous solutions, the ionisation of reactive silanol groups (—SiOH) causes the appearance of charges on the particle surface. The surface charge density and potential are influenced by pH and ionic strength of the surrounding solution. At pH above a certain value (isoelectric point), the surface will become negatively charged thanks to the following reactions:

$$—SiOH + OH^- \rightleftharpoons —SiO^- + H_2O \quad (2\text{-}1)$$

At lower pH values, the free protonated water reacts with silanol groups and form positive groups according to the following reaction:

$$—SiOH + H_3O^+ \rightleftharpoons —SiOH_2^+ + H_2O \quad (2\text{-}2)$$

a

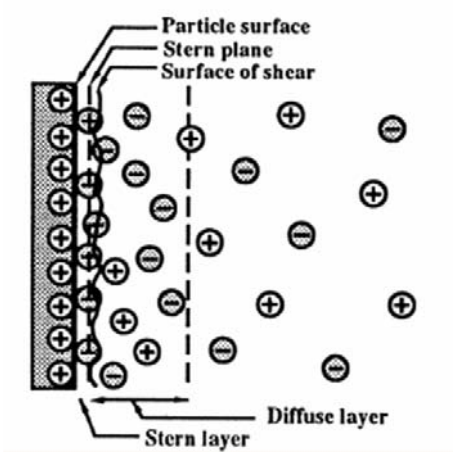

b.

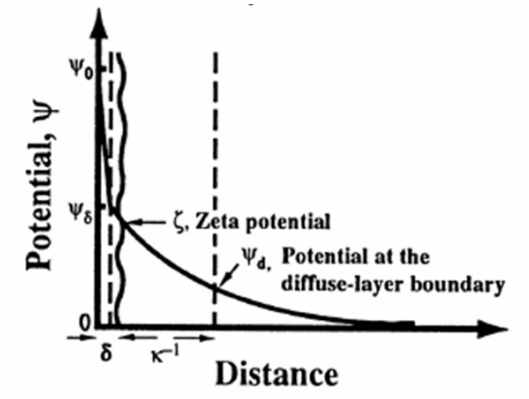

Figure 2-1 Schematic illustration of (a) the electric double layer at a charged surface and (b) the variation of potential with distance from the charged wall [7]

Electric double layer

When a charged surface is present in an aqueous solution, the particle charges are influenced by the ionic strength in the solution. Counter ions will be distributed around the particles and form an electrical double layer consisting of an inner layer and a diffuse layer. In the inner layer, or the so-called Stern layer, counter ions are adsorbed strongly enough to overcome thermal agitation [19]. In the diffuse layer the counter ions are more loosely bound and can be affected by electrical forces and random thermal effects, as shown in Figure 2-1a. When the particles move in solution, a shear plane exists where the counter ions move together with the particles. The potential at this shear plane called the zeta potential (Figure 2-1b), and this is of help to evaluate the inter-particle interactions, surface charge and stability of suspensions. The zeta potential can be determined experimentally by measuring the electrophoretic mobility.

2.2.2 DLVO theory

The first theory concerning dispersion stability, proposed by Derjaguin, Landau, Verwey and Overbeek [20, 21], is known as the DLVO theory. It describes colloidal interactions between particles in a medium by considering the particle interaction energy:

$$\phi = \phi_R + \phi_A \qquad (2\text{-}3)$$

where ϕ_A and ϕ_R represent inter-particular attraction and repulsion, respectively. The attractive forces will always be present and are accounted for by the long-range van der Waals forces, which have their origin in dipole or induced dipole interactions.

The attractive and repulsive interactions depend highly on the distance between the particles. Conventionally the repulsive potential energy is defined as positive while the attractive energy is defined as negative. Figure 2-2 illustrates the potential energy between two particles as a function of the particle separation.

For two spherical particles with equal charge, the electrostatic repulsive interactions in an aqueous medium can be expressed as follows [19]:

$$\phi_R = \frac{32\pi\varepsilon\varepsilon_0 a k^2 T^2 \gamma^2}{e^2 z^2} \exp(-\kappa H) \qquad (2\text{-}4)$$

where

$$\gamma = \frac{\exp(ze\varphi_d / 2kT) - 1}{\exp(ze\varphi_d / 2kT) + 1} \tag{2-5}$$

a is the particle radius, φ_d is the potential energy at the Stern layer, H is the distance between the Stern layers, ε_0 is dielectric constant in vacuum, ε is the relative dielectric constant to vacuum and k, T and e are Boltzmann's constant, absolute temperature and charge of an electron, respectively.

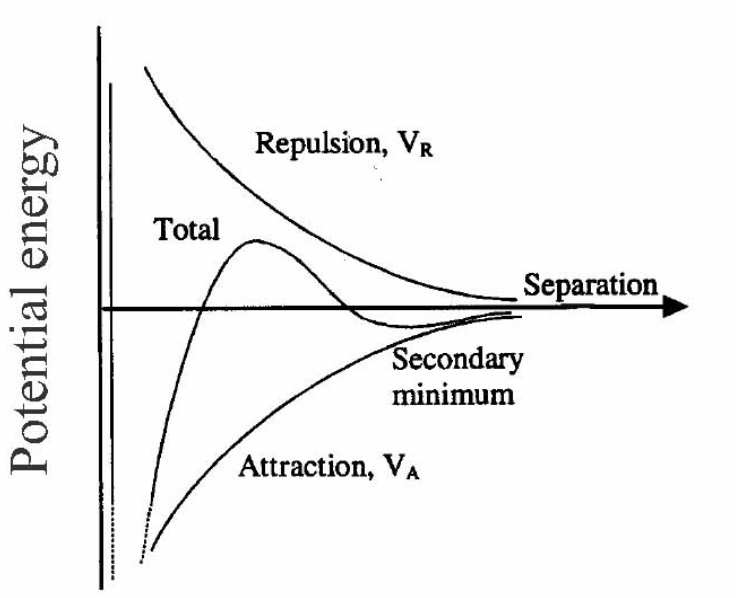

Figure 2-2 Example of potential energy between two particles as a function of separation distance

The van der Waals interaction is expressed as follows [19]:

$$\phi_A = -\frac{A}{12}\left[\frac{1}{x(x+2)} + \frac{1}{(x+1)^2} + 2\ln\left(\frac{x(x+2)}{(x+1)^2}\right)\right] \tag{2-6}$$

where $x = H/2a$, and A is the Hamaker constant. When calculating the DLVO interaction between colloidal particles, it is necessary to evaluate the Hamaker constant: [22]

$$A_{131} = \frac{3}{4}kT\left(\frac{\varepsilon_1 - \varepsilon_3}{\varepsilon_1 + \varepsilon_3}\right)^2 + \frac{3h\nu_e(n_1^2 - n_3^2)^2}{16\sqrt{2}(n_1^2 + n_3^2)^{3/2}} \quad (2\text{-}7)$$

where A_{131} is the Hamaker constant, the subscripts 1 and 3 indicate solid (silica) and the medium (water). *h* is the Planck's constant, ν_e *is* mean value of the UV absorption frequency of silica and the medium, and *n* is the refractive index.

2.2.3 non-DLVO repulsion

DLVO theory successfully explains the colloidal stability of systems in which the attraction is dominated by van der Waals forces, and the repulsion is dominated by electrostatic interactions. However the classical DLVO theory has its limitation: it is applicable only for lyophobic colloids whose advancing contact angle (θ_a) is in the range of 15^o-64^o. DLVO theory fails to describe the surface forces when very hydrophilic ($\theta_a<15^o$) and very hydrophobic ($\theta_a>64^o$) particles are suspended in water. Indeed direct measurement of surface forces with surface force apparatus (SFA) and AFM confirmed the existence of repulsive forces not considered in the DLVO theory [22-25].

For hydrophilic silica ($\theta_a<15^o$) suspended in water, the force is dominated not by van der waals attraction at short range (<3nm), but by non-DLVO repulsion, referred to as structural force such as hydration force. The classical DLVO theory may be extended to include the hydration potential energy (ϕ_H):

$$\phi_t = \phi_R + \phi_A + \phi_H \quad (2\text{-}8)$$

The hydration energy can be described by an empirical double –exponential function of the form:[26]

$$\phi_H = \frac{a}{2}\left(C_1 D_1 \exp(-H/D_1) + C_2 D_2 \exp(-H/D_2)\right) \quad (2\text{-}9)$$

Where C_1 and C_2 are the constant coefficients, and D_1 and D_2 are the decay lengths.

This empirical double –exponential equation has been successfully used to fit the measured short-range hydration forces between the surfaces of solids in water (silica, mica, rutile).[22, 26-28]

Total potential energy curves from the extended DLVO and classical DLVO theory in the case of fumed silica particles (r=6nm) in 0.01M NaCl solutions are shown in Figure 2-3.

Electrostatic repulsions predominate at intermediate distances, the van der Waals attraction will predominate at small, while at short range (<3nm), the hydration force may dominate, and accordingly repulsion interactions (electrical repulsions and hydration) exceed attractive force, which give rise to an energy barrier which is higher than that obtained with classical DLVO.

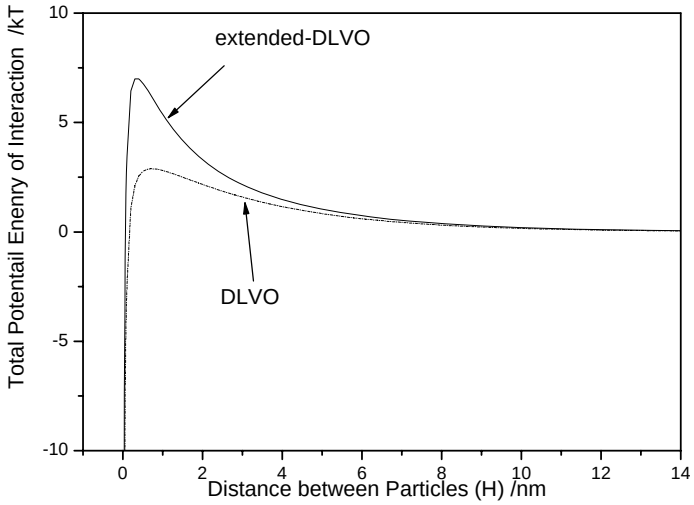

Figure 3 Potential energy curves of extended and classical DLVO theory in case of silica particles (r=6nm) in 0.01M NaCl solutions.

The relative magnitude of the above interactions governs the stability of suspensions as well as their rheological behavior [29-31]. A suspension is stable when the repulsive forces dominate, while the presence of strong attractive forces cause particle aggregation. pH and ionic strength are factors that will influence the relative magnitude of attractive and repulsive forces.

3 Crude oil, Wax and Emulsion

Crude oils are complex fluids that can cause various difficulties during the production, separation, transport and refining of oil [32-34]. Wax formation and deposition are some of the problems that can be encountered [35-37]. Indeed below a critical temperature, wax crystals start to precipitate as the solubility of high molecular weight paraffins decreases, and the flow properties of the oil change. Another problem arises from emulsion formation. Indeed, crude oil is often mixed with water when it comes out from a well. As the oil/water mixture passes over chokes and valves mechanical input leads to the formation of water-in-oil (W/O) emulsions [38]. Such emulsions are a relentless problem within the petroleum industry as they give rise to a variety of costly problems in terms of production loss, transport difficulties and chemical expenses. The chemistry behind the phenomena of crude oils, waxes and emulsions is primarily concerned in the following sections.

3.1 Crude oil composition

A crude oil is a complex mixture of chemical compounds composed mainly of carbon and hydrogen with small amount of other nonmetallic elements such as sulfur, oxygen, and nitrogen, as well as trace amounts of metallic constituents, particularly vanadium, nickel, iron and copper [32]. Although the crude oil composition may vary widely from its origin, the carbon and hydrogen contents vary over narrow limits, carbon content is normally between 83 and 87% and the hydrogen one in the range 10-14% [32].

Due to thousands of chemical compounds present in crude oil, complete defining of the structure and composition of each individual molecule seems impossible. It is a practical and frequently employed way to divide crude oils into different fractions with respect to their polarity and solubility [39-43], which is known as SARA separation. In this method, the SARA-separation scheme is displayed in Figure 3-1. The crude oil system is isolated into four groups of Saturates, Aromatics, Resins and Asphaltenes.

Saturates are, by definition, non-polar hydrocarbons including straight and branched alkanes, as well as cycloparaffins compounds (naphtenes). Wax which mainly consists of the long chain paraffins is believed to be a sub-class of saturates. Aromatics refer to all compounds with one or more aromatic nuclei which may be linked up with naphtene rings and/or

aliphatic side chains. Saturates and aromatics generally are the lightest fractions of the crude oil [5, 32].

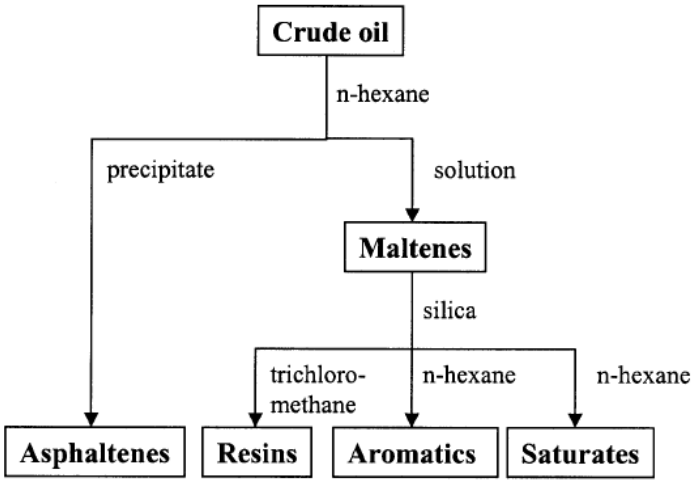

Figure 3-1 SARA-separation scheme [44]

Resins are defined as polar molecules often containing heteroatoms such as nitrogen, oxygen or sulfur. This fraction is soluble in light alkanes such as n-heptane or n-pentane but insoluble in liquid propane [32, 45]. Asphaltenes are defined in terms of a solubility class that is precipitated from petroleum by the addition of an excess of a light alkanes like pentane, hexane or heptane. The precipitate is soluble in aromatic solvents like toluene and benzene [33, 45, 46]. Asphaltenes are the heaviest, most aromatic components of crude oil with the largest percentage of heteroatoms (O, S, N) and major part of organometallic constituents (Ni, V, Fe) in the crude oil. The structure of a hypothetical asphaltene monomer molecule is illustrated in Figure 3-2.

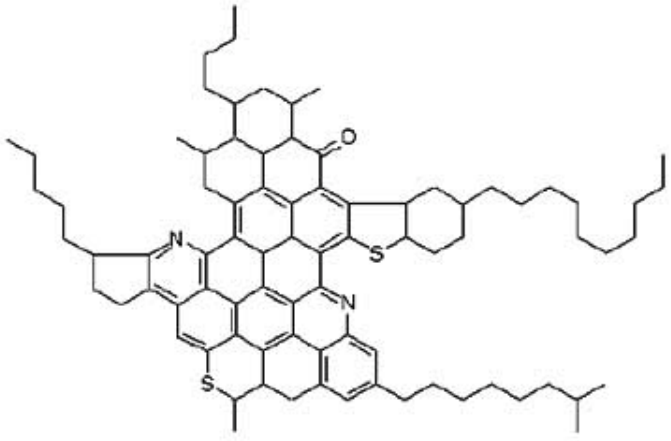

Figure3-2 Structure of a hypothetical asphaltene monomer molecule [47, 48]

Asphaltenes have been extensively studied because of their enormous impact on petroleum production, transportation and refining. Generally, asphaltenes increases stability of W/Crude oil emulsion, an issue of growing influence in oil transportation and separation. Self-association and precipitation of asphaltene particles in oil system may make problems in the pipeline and oil well. Efficient processing of asphaltic oils has been and remains a big challenge in petroleum refining industry [32, 34].

Due to asphaltenes tendency to self-associate, it is difficult to exactly determine asphaltene molecular weights. Many factors may influence the self-association of asphaltenes. Non-polar solvents and pressure reductions may promote asphaltene aggregation [5]. Because of these difficulties, a wide range of asphaltene molecular weights from a few hundreds to several millions have been reported [4, 32]. Lately, a good estimate of the asphaltene monomer mean molecular weight of approximately 750 g/mole have been reported [49]. The diameter of asphaltene monomers have been reported to be in the range 10-20 Å [49, 50].

3.2 Emulsion

An emulsion is a mixture of two immiscible liquids in which fine droplets of one liquid (the dispersed phase) is dispersed in another (the continuous phase), as droplets of colloidal sizes (~ 0.1-10 μm) or larger [51]. Emulsions are of great concern due to their widespread occurrence in everyday life and industry. The various emulsions occurring in everyday life may be desirable. Examples of emulsions include butter and margarine, cosmetics and pharmaceutical as well. Emulsions are also frequently encountered in the petroleum industry, where they are typically undesirable. Indeed, the formation of water-in-oil (W/O) emulsions may cause production loss and transport difficulties.

In the definition of emulsion stability, the break-up mechanism involves three different processes: flocculation, sedimentation (creaming) and coalescence [51]. Sedimentation and creaming result from a density difference between the two liquid phases and is promoted by large droplet sizes, high differences in density and low viscosity of the continuous phase. The velocity of sedimentation/creaming (u) in dilute systems can be described with Stokes equation [52].

$$u = \frac{2(\rho_w - \rho_o)gr^2}{9\eta_o} \qquad (3\text{-}1)$$

Where ρ_w and ρ_o are density of dispersed and continuous phases, respectively. *r* is the radius of dispersed droplet. η_o is viscosity of continuous phase. *g* is the acceleration due to gravity.

Flocculation is a reversible formation of droplet clusters where two or more droplets clump together, touching only at certain points and with virtually no change in total surface area. In flocculation the individual droplets retain their size and shape, but lose their kinetic independence because the aggregate moves as a single unit. Formation of flocculates will increase the sedimentation/creaming rate.

Processes of creaming, sedimentation and flocculation are all reversible. Application of agitation will promote the recovery of original dispersion state. A much more severe phenomena is coalescence, the complete mergence of two bubbles into one. Processes that facilitate the coalescence are film drainage and film rupture. The mechanisms are illustrated in Figure 3-1[52].

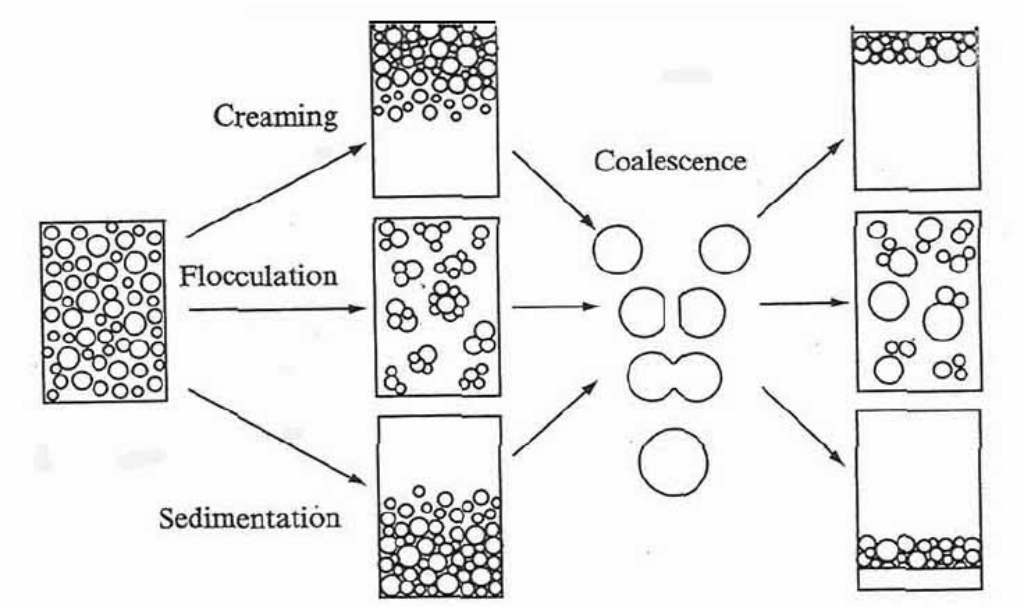

Figure 3-1 Illustration of emulsion breakdown and separation processes [52]

The properties of the interface between water and oil are vital in determining the stability of an emulsion system. The formation of interface between the dispersed phase and the continuous phase increases the system free energy, therefore the emulsions are not thermodynamically stable, and tend to minimise the surface area by break-up of emulsions. If the interfacial film is weak, the emulsions stability will be poor. The dispersed droplets will collide and the collisions will lead to droplet fusion, i.e. coalescence.

Many studies have been carried out to improve the understanding of the stabilisation/destabilisation mechanisms of crude oil emulsions [53-59]. Indigenous amphiphilic substances in the crude oil, i.e., asphaltenes and resins, are traditionally considered as natural emulsifiers responsible for the stabilization of W/O emulsions. Formation of rigid, three-dimensional films of asphaltene aggregates at the oil-water interface is believed to protect water droplets from coalescence. In addition waxes, fine solids (e.g. scale, sand and clay) and naphthenates may contribute to the film strength at the oil/water interface. Furthermore, the stability of emulsions also depends on the aggregation state of asphaltenes [38, 60-64].

3.3 Wax

The presence of long-chain saturated alkanes in crude oil can lead to severe problems associated with wax precipitation and deposition in petroleum transport pipelines and processing equipments [35, 65, 66]. Indeed, the paraffin deposition on the cold walls of pipelines will restrict the flow, and in the worst case entirely plug the pipelines. Figure 3-2 shows the wax plugging in a cut-away segment view of a pipeline [3].

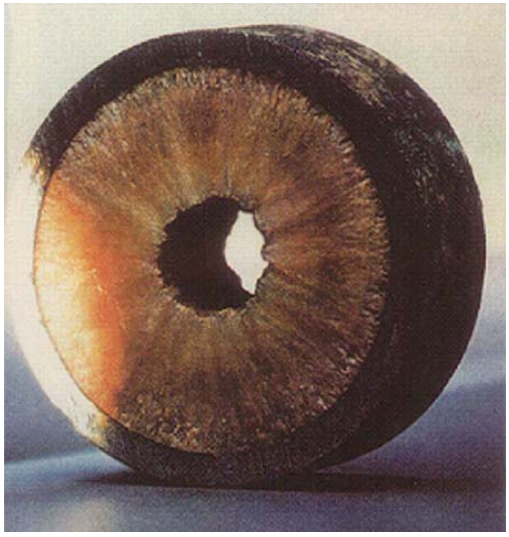

Figure 3-2 Cross-sectional view of a plugged pipeline [3]

Secondly, presence of solid waxes in continuous oil systems may give rise to the difficulty of prediction and evaluation of the flow properties [35] which is largely dependent on the waxy constituents of the oils.

Different from oil fields to oil fields, waxes have a broad molecular weight distribution ranging approximately from 10 to 100 carbons or even higher. Waxes are typically classified

as straight-chain n-alkanes/paraffin (C20-C40), and microcrystalline consisting of high molecular weight isoparaffins and cycloparaffin. (Figure 3-3).

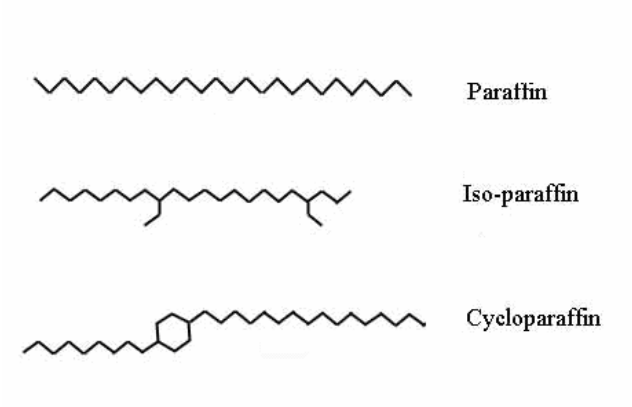

Figure 3-3 Molecular structures schematics of three kinds of waxes

Paraffins generally crystallize as large needles and plates due to the straight-chain compounds which can regularly array, while microcrystalline is termed amorphous wax, mainly consisting of branched and cyclic hydrocarbons [35]. Crude oils generally contain not only n-paraffins but also considerable amounts of isoparaffins and cyclic compounds, which in fact constitute the largest fraction [35]; Visintin et al. [67] found that n-paraffin dissolved in organic solvents display a sharp transition in gel strength at the pour point, whereas by addition of isoparaffins, the buildup in gel strength as a function of temperature is much more gradual, because increasing isoparaffin fraction facilitates the formation of amorphous wax solids.

At high temperatures, waxes are in the molten state, and crude oils normally behave like Newtonian liquids. When the temperature drops below Wax Precipitation Temperature (WPT), solid wax crystals precipitate out of oils and form a gel. In the definition of wax crystallization at a more microscopic level, the gelation mechanisms involves three different processes: formation of lamellar with thicknesses of ca. 1.5-3 nm [67-69] , sheet-like crystals, micrometer-size structure, and the final large network gel.

Crystallization of paraffins also depends on physical factors (cooling rate, shear force and so on). The length of the crystals is dependent on the temperature and cooling rate [70]. Kane et al. studied the growth wax crystal in crude oils under quiescent and shearing conditions with TEM [68]. They found that shear forces prevent gelation by blocking lateral growth of the individual disks. The crystal aggregation is also very sensitive to the shear rate. At static condition, individual disks form a colloidal network. At high shear rates, the aggregates become more spherical in shape and less distributed in size.

4 Rheology

Dispersions can respond in different ways to a deformation [71]; they can be viscous, elastic, or viscoelastic. It is the goal of rheology to study these responses.

4.1 Theory

The basic principles and common models used in rheology are briefly introduced in the following sections.

4.1.1 Basic variables

Rheolgy is the science which focuses on the deformation of matter resulting from the application of a force [51]. The force can be applied in various ways: as a tension, a compression, a shearing process, or some combination of three. One simple type of deformation, shear, is illustrated in Figure 4-1 [51]. The lower plate of two parallel ones is held stationary. The upper plate is pulled with a velocity U with respect to the lower one. The applied shearing force is F, acting in the *x* direction over area A. The space between the planes is filled with a sheared fluid and the lengths of the arrows between plates are proportional to the local velocity in the fluid. With consideration of simple laminar flow, we can define the basic parameters as the following:

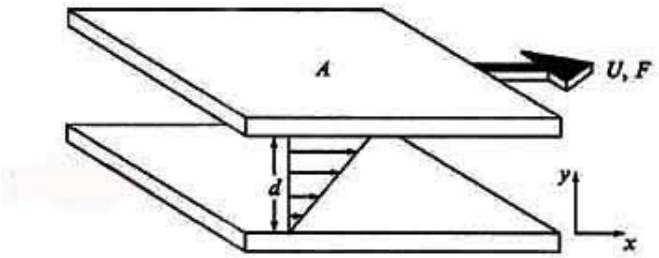

Figure 4-1 Deformation of a liquid under an applied shear force F [51]

Shear stress is defined as the forced divided by the area over which it is applied:

$$\tau = {}^{dF}\!/_{dA} \qquad \text{in Pa} \qquad (4\text{-}1)$$

Shear strain is the relative deformation per unit length. The length is the one over which the deformation occurs.

$$\gamma = {dx}/{dy} \qquad \text{dimensionless} \qquad (4\text{-}2)$$

Shear rate is the speed of deformation:

$$\dot{\gamma} = {d\gamma}/{dt} \qquad \text{in s-1} \qquad (4\text{-}3)$$

Simple liquids are generally Newtonian, that is to say the shear stress is proportional to the shear rate. It is easy to describe such materials with a simple linear equation,

$$\tau = \eta\dot{\gamma} \qquad (4\text{-}4)$$

where η is named viscosity, with unit Pa $s^{-1.}$

Another simple case is the one of pure elastic material in which the stress follows the Hookean law with respect to strain:

$$\tau = G\gamma \qquad (4\text{-}5)$$

Where G is elastic modulus, with unit Pa.

The majority of dispersions shows complex rheological behaviours intermediary between Newtonian and Hookean ones defined as viscoelatic. These materials can be modelled as various combinations of Hookean springs and Newtonian dashpots. Two simplest models are the Maxwell model and the Kelvin model, in which the spring and dashpot are arranged in series and parallel, respectively. (Figure 4-3) [71]

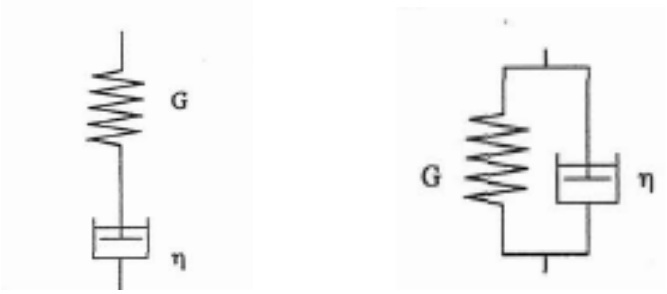

Maxwell model: Kelvin model:

$$\tau=G\gamma+\eta\dot{\gamma} \qquad (4\text{-}6) \qquad\qquad \dot{\gamma}=\frac{\tau}{G}+\frac{\tau}{\eta} \qquad (4\text{-}7)$$

Figure 4-2 Two simplest viscoelastic models: Maxwell model and Kelvin model [71]

It exits several tests to characterize rheological features of materials. In the following, we will describe the most known.

4.1.2 Steady shear flow

In this test, fluids are studied by subjecting them to continuous shearing at constant rate. We introduce the apparent viscosity with the following formula:

$$\eta_{app} = \frac{\tau}{\dot{\gamma}} \qquad (4\text{-}8)$$

The evaluation of shear stress with the shear rate for materials can be described by several behaviours. (Figure 4-3).

----Newtonian fluids: the apparent viscosity is independent of the shear rate.
----Shear thinning (pseudoplastic) fluids: These fluids present a decrease of the apparent viscosity when the shear rate increases.
----Shear-thickening (dilatant) fluids: Contrary to the former cases, the apparent viscosity of these fluids increases with the shear rate.
----Bingham plastic fluids: An important characteristic of these materials is the presence of a yield stress τ_0. Below this yield stress, a material exhibits solid like characteristics, and we must apply a yield stress above this value to make the material flow.

Flow curves of Non- Newtonian materials can be described by some equations, a short description of them is as follows:

Power law equation for pseudoplastic or dilatant fluids:

$$\tau = K\dot{\gamma}^n \qquad (4\text{-}9)$$

Where K is the consistency coefficient (also called viscosity), and n is the power law index.

Bingham model:

$$\tau = \tau_B + \eta_p\dot{\gamma} \qquad (4\text{-}10)$$

It can be used to describe the plastic behaviours with a linear equation. where η_p is the plastic viscosity and τ_B is the yield stress. Yield stress is an important property for the restart of transport. It is the upper limit of shear stress before flow occurs, at which point that the

range of reversible elastic deformation ends and range of irreversible deformation or viscoelastic- viscous flow begins [71].

The Herschel-Bulky model for pseudoplastic or dilatant fluids with yield stress:

$$\tau = \tau_0 + K\dot{\gamma}^n \qquad (4\text{-}11)$$

Where τ_0 is the yield stress.

A further model to characterize non-Newtonian fluids is the Casson model:

$$(\tau)^{0.5} = (\tau_0)^{0.5} + K(\dot{\gamma})^{0.5} \qquad (4\text{-}12)$$

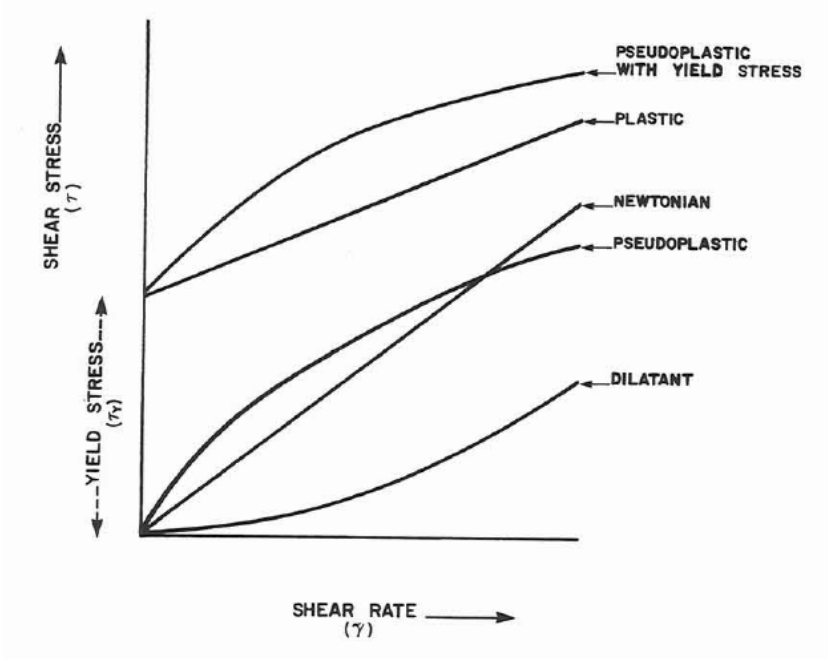

Figure 4-3 Newtonian and non- Newtonian phenomena [8]

4.1.3 Oscillation response

This test allows us to study viscoelastic properties of materials without disturbing their bulk structure.

In this test, for linear viscoelastic materials, if an oscillating strain is applied at a given pulsation (ω) with a deformation amplitude γ_0: (Figure 4-4. [71])

$$\gamma(t)=\gamma_0 \sin(\omega t) \qquad (4\text{-}13)$$

This vibration movement results in a time-dependent shear stress having a phase shift $-\delta$,

$$\tau(t)=\tau_0 \sin(\omega t-\delta) \qquad (4\text{-}14)$$

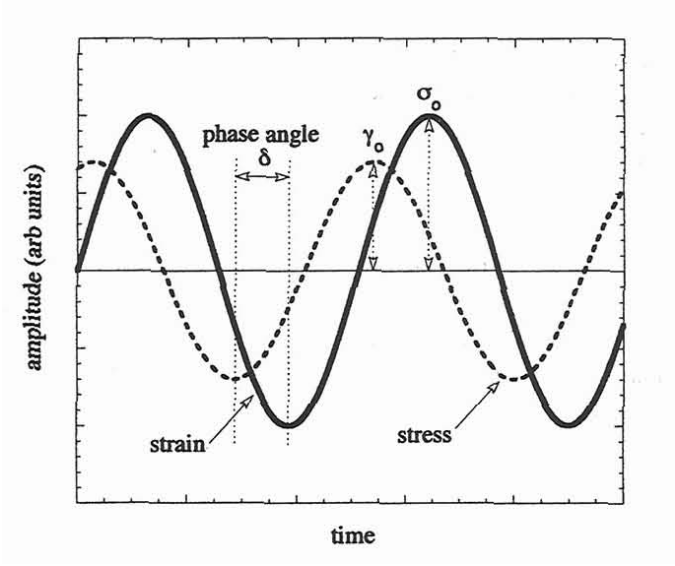

Figure 4-4 An oscillating strain and the stress response for a viscoelastic material [71]

An important term, complex modulus G*, is defined as the ratio of the maximum stress τ_0 and the maximum strain γ_0:

$$\left|G^*(\omega)\right| = \frac{\tau_0}{\gamma_0} \qquad (4\text{-}15)$$

Complex modulus G* is constant for a given radial frequency ω. The storage and loss moduli are derived from the phase angle and complex modulus:

$$G'(\omega) = G^*(\omega)\cos(\delta) \qquad (4\text{-}16)$$

$$G''(\omega) = G^*(\omega)\sin(\delta) \qquad (4\text{-}17)$$

The storage and loss moduli are subtle descriptions of the viscoelastic properties and microstructure of the system, *G'* is a measure of the energy which is stored during the vibration procedure. If *G'*= 0, the sample is a purely viscous fluid. *G''* represents the energy, dissipated during the vibration procedure. If *G''*= 0, the sample is a Hookean fluid.

We define:

$$tg\delta = \frac{G''}{G'} \qquad (4\text{-}18)$$

as the damping factor.

These above parameters (damping factor, storage and loss moduli) are frequency-dependant.

4.1.4 Creep-recovery

Creep–recovery method is also very useful to investigate the viscoelasticity. The creep-recovery experiments were conducted as the following: A constant shear stress (τ_0) starts to apply on the sample at time $t_{0,}$ and the resulting strain was monitored as a function of time. The imposed stress was suddenly removed at time t_1 and recoverey, on release of the stress was monitored until time t_2. (Figure 4-5)

The fluid response is characterized by two phases, the creep phase and the recovery phase. In the creep phase, the time dependence of creep compliance $J(t)$ can be given by

$$J(t)=J_0+J_r(t)+J_v(t) \qquad (4\text{-}19)$$

where J_0 is the instantaneous compliance, $J_r(t)$ is the retardation compliance, and $J_v(t)$ is the viscous flow compliance. $J_r(t)$ represents the delayed elastic compliance and gradually increases with time. The viscous flow compliance, $J_v(t)$, represents the irreversible component of compliance and increases gradually with time.

The creep phase can be modelled using either the Maxwell fluid model or the Burger model depending upon the availability of $J_r(t)$. The Maxwell model consists of a spring with modulus G_0 and dashpot with viscosity η_0 placed in series (Figure 4-6), and is response to the creep test is the following [72]:

$$J(t) = \frac{1}{G_0} + \frac{t}{\eta_0} \qquad (4\text{-}20)$$

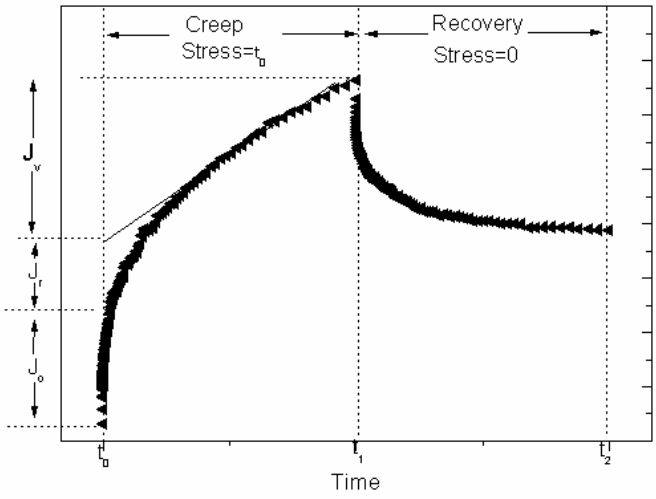

Figure 4-5 Schematics of Creep–recovery curve

The Burger model consists of two springs with moduli G_0 and G_1 and two dashpots with viscosities η_0 and η_1 (Figure 4-6) [73] and can be described by the mathematical model as:

$$J(t) = \frac{1}{G_0} + \frac{t}{\eta_0} + \frac{1}{G_1}\left[1 - \exp\left(\frac{-G_1 t}{\eta_1}\right)\right] \qquad (4\text{-}21)$$

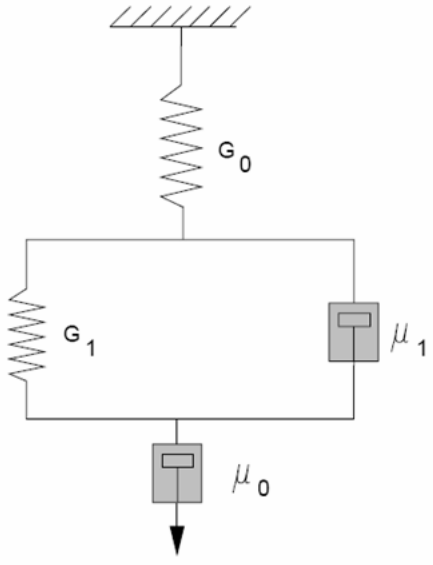

Figure 4-6 Four element Burger model [73]

4.2 Rheology of dispersions

The rheological properties of particle suspensions are of great importance in numerous industrial applications such as paints and coatings, ceramics, coal and well drilling slurries, etc [9-12]. Concentrated suspensions display different rheological behaviours than Newtonian fluids, as they can be shear thinning, shear thickening, thixotropic, rheopectic, and viscoelastic.

Forces that can occur in particle suspensions have been investigated by Zeman et al.[30], and can be summarised as hydrodynamic, colloid chemical, Brownian movement, gravitational, inertial, and electroviscous. Some of these forces have already been presented in Section 2.2. Of which, colloidal forces determine the particle interaction during deformation and consequently the microstructure and the rheological behaviours of dispersions. Hydrodynamic forces include the viscous drag force and particle–particle interactions resulting from the perturbation of the presence of solid particles in the flowing medium. In addition to colloid chemical forces, hydrodynamic forces become predominant in the resistance to flow and deformation of concentrated suspensions, while the size-dependent Brownian movement become more significant at lower volume fractions [30].

4.2.1 Hydrodynamic forces

The most important variables that influence Hydrodynamic forces include: volume fraction of solids, the particle shape, size and size distribution of particles, the surface and mechanical characteristics, and the fluid properties [30].

4.2.1.1 Volume Fraction

The volume fraction affects both the viscous and viscoelastic behaviour of dispersion systems. The dilute suspensions have a random, isotropic structure which does not change significantly with increasing shear rate. In contrast, at high volume fraction, particles are close enough for packing, interlocking and structure formation. Then the solid particles do not move at random anymore, but will form agglomerates, which is responsible for shear thinning or thickening phenomena. Increasing of viscosity due to volumetric effects is pronounced in concentrated suspensions [30]. The evolution of viscosity with association to volume fraction will be discussed in detail below.

For dilute hard sphere suspensions ($\phi < 0.05$), Einstein's equation predicts the relationship between volume fraction and viscosity:

$$\eta = \eta_0 (1 + 2.5\,\phi) \qquad (4\text{-}22)$$

where η and η_0 are the viscosity of the suspensions and the suspending fluid, respectively and ϕ is the particle volume fraction.

For concentrated hard sphere suspensions, the semi-empirical Krieger and Dougherty equation [74] was employed to define the relative viscosity as a function of volume fraction:

$$\eta_r = \eta / \eta_0 = (1 - \frac{\phi}{\phi_m})^{-[\eta]\phi_m} \qquad (4\text{-}23)$$

where η_r is the relative viscosity of suspensions with respect to the fluid, ϕ_m is the maximum packing fraction, and $[\eta]$ is the intrinsic viscosity of suspensions.

Mooney [75] proposed another equation to describe the relationship between the relative viscosity and the volume fraction of solid particles:

$$\eta_r = \eta_\infty / \eta_0 = EXP\left(a\phi / (1 - \phi / \phi_m) \right) \qquad (4\text{-}24)$$

where a is a coefficient, η_∞ is the higher limiting shear viscosity and ϕ_m is the maximum packing fraction.

When ϕ approaches zero, which means very dilute systems, the Mooney equation will approach the Einstein equation. At increasing concentration, the crowding of particles around that concentration results in an interlocking, preventing the suspension from flowing, and finally reaching the maximum packing. The theoretical value of maximum packing fraction is 0.74 for a close-packed array of same size spheres. Jeffrey suggested that a is an Einstein constant with value between 2.5 and 5.0 [76].

4.2.1.2 Particle size

Both size and size distribution of particles can be of primary importance because it determines collisions and packing. The higher viscosity at a given volume fraction for the

smaller particle sizes is due to shorter interparticle distance and consequently the interactions between the particles are stronger as compared with larger particles. Then the shear thinning effects become more pronounced as the particle size decreases [77-81].
As compared with monodisperse systems, wider size distribution may give rise to a much closer packing and higher values of maximum packing [78, 81, 82]. The shifts are mainly due to that small particles can fill the interstices between the large ones and consequently reduce the relative viscosity at fixed volume fraction [83]. The decrease becomes more pronounced with increasing volume fraction and with the increasing aspect ratio R, of the large over the small diameter.

4.2.1.3 Shape and deformation

Generally, complex particle geometry leads to the decreasing of maximum packing fraction [82]. For rod or fiber shape particles with a high aspect ratio of 20, maximum packing fraction is only 0.2 [84, 85]. The orientation and deformation must also be under consideration for complex-shape particles, soft particles and flocs or aggregations. Complex shape particles tend to align in the flow direction. Soft surface particles including emulsions droplets may deform as axisymmetric particles along the plane of shear. The presence of flocculates will increase the viscosity. Application of stresses will promote particles alignment in the direction of shear and break down the structure of floc/aggregates [51]. (Figure 4-7).

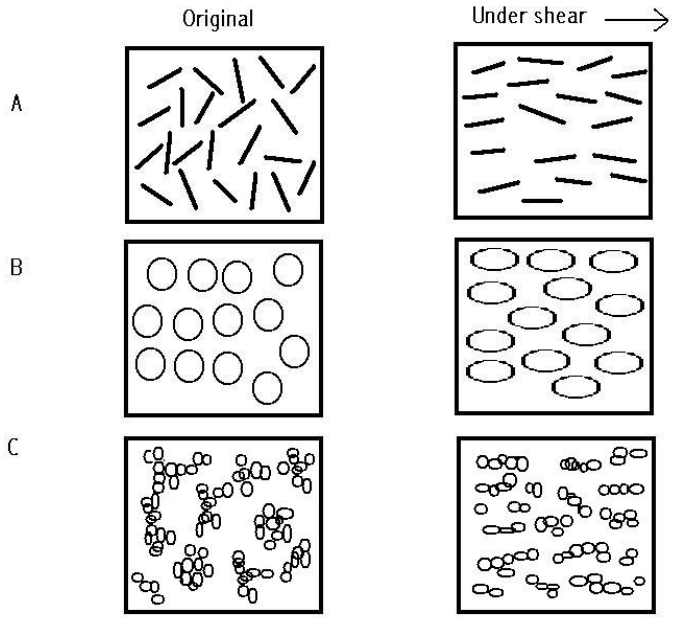

Figure 4-7 Illustration of deformation, orientation and structure break-up phenomena during flow for rod-like particles (A), Soft particles (B) and flocs or aggregations (C).

4.2.2 Colloidal forces

The rheological behaviour of dispersions depends on the interparticle interaction, consequently the factors that influence colloid chemical forces should be considered: the species adsorbed on their surfaces, the nature of the liquid medium and so on [80, 81]**.**

As discussed in particle interaction part (section 2.2), a suspension will be stable when the repulsive forces dominate, while the presence of strong attractive forces will cause particle aggregation. The parameters influence colloidal chemical forces can be ranked into two categories:

Forces which govern electrostatic interactions between particles: for instance: pH, ionic strength, particle surface charges and so on.

Presence of macromolecules: If these macromolecules are absorbed on the particle surface, they will generally stabilize them by steric repulsions. But if it is not the case, they could induce flocculation of particles.

If the particles are stable, the suspensions would be low viscous. Whereas, if there is strong flocculation, suspensions would present a very high viscosity, and generally shear thinning and thixotropy. If the level of flocculation is moderate, depending on the balance between repulsive and attractive forces, different levels of flocculation and therefore varying rheological properties can be obtained.

4.2.3 Brownian movement

In practice, particles suspended in a liquid are never stationary. The particles are constantly moving due to Brownian motion. Brownian motion is the movement of particles due to the random collision with the molecules of the liquid that surrounds them. Small particles move quicker than the large particles. In suspension rheology, Brownian movement is of direct importance to the smaller diameter of the particles in dilute dispersion.

Brownian movement entails a tendency towards more random radial and orientational distribution functions, which in turn counteracts the effect of flow. Randomization of the distribution functions due to diffusion brings the dispersion back to a random equilibrium condition, and, as such, provides a “memory” for the equilibrium structure. It ensures a reversibility not present with large particles. At low shear rates Brownian motion dominates and prevents alignment of micrometric particles with respect to the shear plane, resulting in

an equilibrium structure and in Newtonian behaviour. At high shear rates, the convective motion of the flow dominates, affects the structure and results non-Newtonian, shear-thinning, behaviour which appears in a situation similar to that of the large particles [86-93].

5 Experimental Techniques

5.1 Contact angle

Contact angle provides information about the ability of a material to wet a solid and strength of the interaction between solids and liquids. By definition, the contact angle is the angle between the surface and a line that is tangent to a drop of liquid on the surface at the point where it intersects the surface. (Figure 5-1) [51] [94, 95]

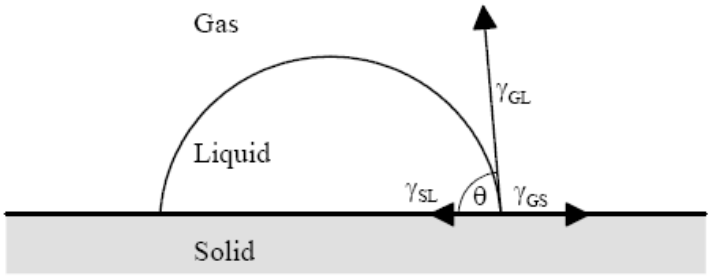

Figure 5-1 Schematic diagram of a contact angle

The force balance on the three phase contact line is given by Young's equation [51, 95]:

$$\gamma_{GL}\cos(\theta) = \gamma_{Gs} - \gamma_{sL} \qquad (5\text{-}1)$$

Where γ_{Gs} is the surface free energy of the solid in contact with gas, γ_{GL} is the surface tension of the liquid-gas interface, γ_{sL} is the surface free energy of the solid covered with liquid, and θ is the contact angle.

However, static contact angle θ_s only results from an equilibrium which requires letting the drop sit on the surface for a long period of time. Often it is practical to measure the contact angle as the drop is expanding (advancing contact angle θ_a) or contracting (receding contact angle θ_r) (Figure 5-2). The relation between these contact angles is given as the following,

$$\theta_a > \theta_s > \theta_r \qquad (5\text{-}2)$$

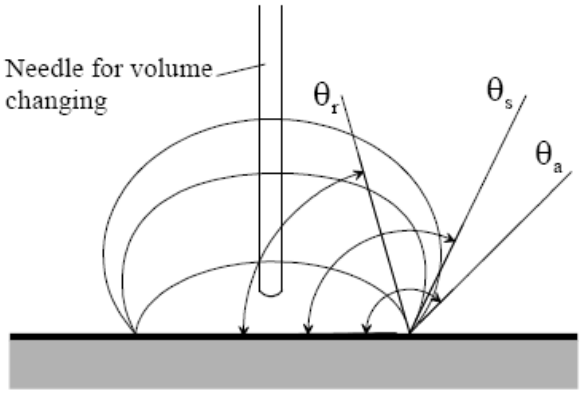

Figure 5-2 Schematic diagram of static contact angle θ_s, advancing contact angle θ_a and receding contact angle θ_r [94]

The Optical Contact Angle Meter (CAM®) equipped with a computer controlled, high speed camera was used to determine the Static advancing contact angles, (Figure 5-3). The sample was pressed into a flat pellet under high pressure, and a series of images of the water droplets on solid surface during the advancing were recorded. The contact angles were determined by fitting the Young-Laplace equation to the drop profile.

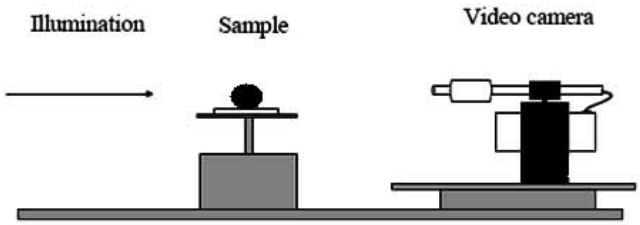

Figure 5-3 Schematic of a contact angle meter [94]

5.2 Zeta potential

The magnitude of the zeta potential indicates the potential stability of a colloidal system. For particles with a large zeta potential magnitude, all the particles in suspension tend to repel each other and there is no tendency to flocculate and vice versa.

In section 2.1, the mechanism of electrical double layer is described. A net charge at the particle surface affects the distribution of ions in the surrounding interfacial region, resulting

in an increased concentration of counter ions close to the surface, (Figure 5-4). The potential that exists at this boundary is known as the Zeta potential.

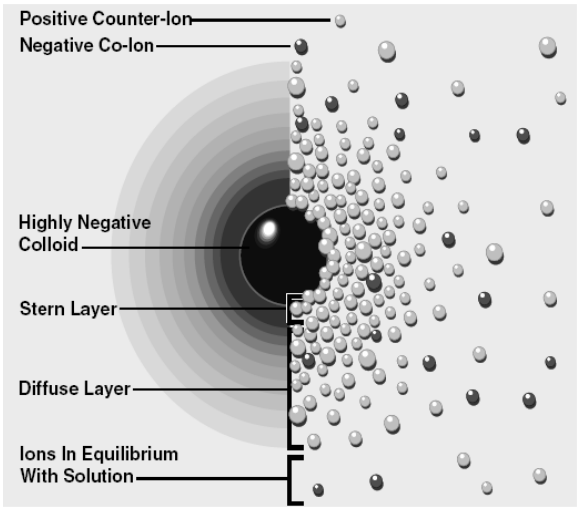

Figure 5-4 Schematic illustration of the electric double layer [8]

The most important factor that affects zeta potential is pH. Generally, a zeta potential versus pH curve will be positive at low pH and lower or negative at high pH. The point where the plot passes through zero zeta potential is called the isoelectric point and is very important from a practical consideration. A typical plot of zeta potential versus pH is shown below, Figure 5-4.

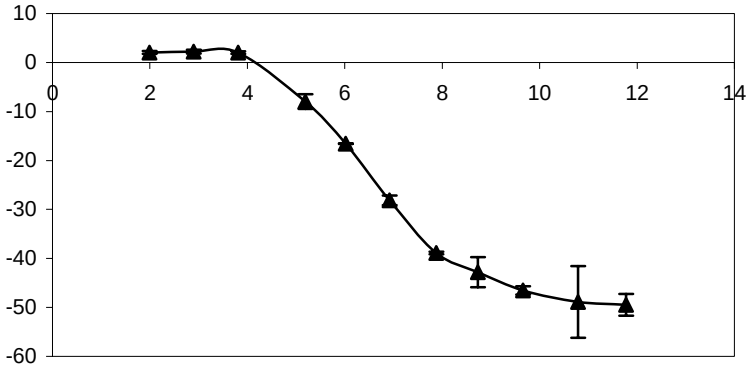

Figure 5-4 Plot of zeta potential versus pH is shown below in the case of fumed silica dispersed in 0.01M NaCl solution

Electrophoresis is a widely used method to measure the zeta potential and is based on the following principles: a charged particles moves in an electrical field with a given speed, and the speed or electrophoretic mobility (u_E) is related with zeta potential (ζ) according to Henry equation [95] [96]:

$$u_E = \frac{\varepsilon \zeta f(\kappa a)}{1.5\eta} \qquad (5\text{-}3)$$

Where η is the viscosity of the solvent, ε is the dielectric constant of the solvent and *f(ka)* is Henry's function, wherein *a* is the particle radius and *k* is the inverse of the electrical double layer thickness.

For spherical particles, aqueous systems with moderate electrolyte concentration solutions, the term f (Ka) is 1.5. So the Smoluchowski approximation is obtained [95],

$$u_E = \frac{\varepsilon \zeta}{\eta} \qquad (5\text{-}4)$$

Laser Doppler Velocimetry (LDV) is a well established technique in studying the mobility of the particles [52]. Figure 5-5 illustrates the Scheme of the Zetasizer® for measuring the zeta potential. First of all, a laser provides a light source to illuminate the particles within the sample; this light source is split to provide an incident and reference beam. The laser beam are crossing at a particular point in the cell, illuminating the passing particles, and the scattering at an angle of 17° is detected. Particles moving through the measurement volume will cause the intensity of light detected to fluctuate with a frequency proportional to the particle speed (Doppler effect). The detector feeds the information to a digital signal processor and computer where the frequency spectrum is determined and consequtenly the zeta potential information is calculated.

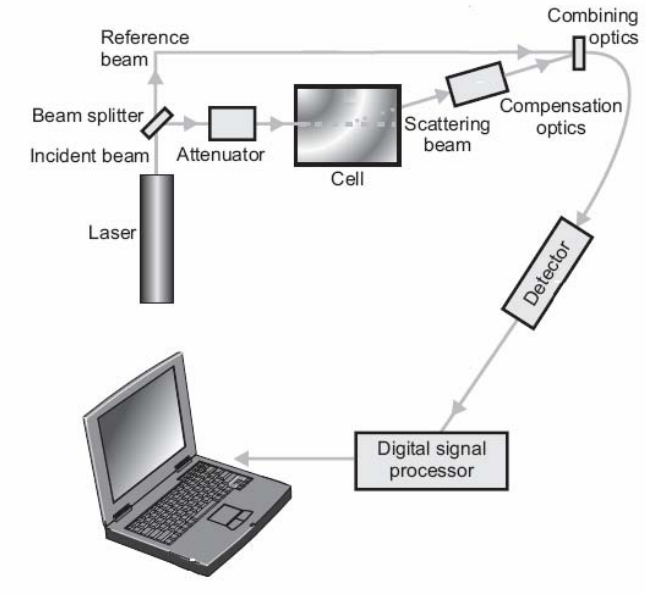

Figure 5-5 Scheme of the Zetasizer for measuring the zeta potential of particles based on electrophoretic mobility.

5.3 Dynamic Light Scattering

Dynamic Light Scattering (DLS) is a very powerful method to determine particle size and particle size distribution of dilute suspensions. It is an indirect method to measure size in the range from 2 nm to 2 μm, in the colloid domain [95]. Comparing with other technique in this size range, the advantages of DLS are significant [95]: DLS measurements are fast, sample preparation is simple, and it records a large number of particles per experiment and consequently avoid the risk of not displaying a representative part of the sample.

Due to Brownian motion, small particles move quicker than large particles do in dilute suspensions. The relationship between the size of a particle and its speed (diffusion coefficient) is defined in the Stokes-Einstein equation.

$$D_T = \frac{kT}{6\pi\eta R_H} \qquad (5\text{-}5)$$

where D_T is translational diffusion coefficient, k is the Boltzmann constant, T is the temperature, η is the solvent viscosity and R_H is the hydrodynamic radius.

Because of Brownian motion of the particles, interference between scattered light produces a time-dependent intensity fluctuation at the detector. The DLS system measures the fluctuation in scattering intensity and then uses this to calculate the rate of decay for the correlation function, which is used to calculate particle size. Details about the dynamic light scattering can be found elsewhere [95].

In a similar way to the typical Zeta potential system described in Section 5.2, a size measurement system (Zetasizer®) comprises of six main components. First of all, a laser beam (usually a He–Ne laser, λ= 633 nm) provides a light source to illuminate the particles within the sample. A detector is used to measure the intensity of the scattered light at 90°. The detector feeds the information to a digital signal processor which compares the scattering intensity at successive time intervals to derive the rate at which the intensity is varying. Finally, the data from correlator is analysed with the Zetasizer software to obtain size information.

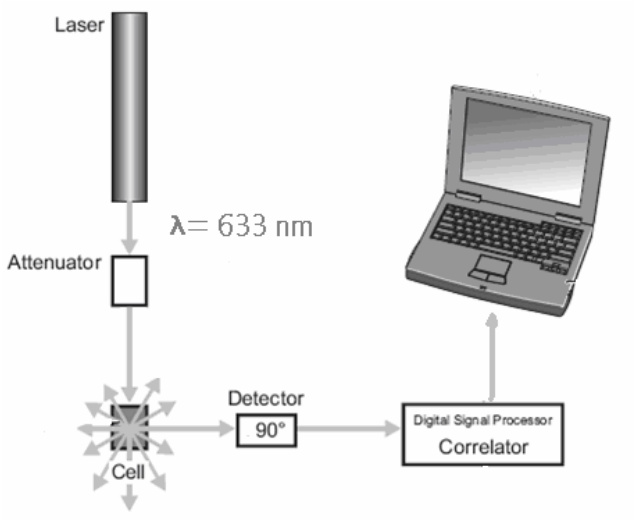

Figure 5-6 Schematic arrangement of the Zetasizer® Dynamic light scattering apparatus

5.4 Differential Scanning Calorimetry

Differential scanning calorimetry (DSC) is a thermoanalytical technique, in which the difference in heat flow between the sample and a reference at the same temperature is recorded as a function of temperature. DSC is commonly used in studies of wax systems in order to determine the onset temperature of wax crystallization as well as the amount of crystallized waxes under quiescent conditions [97-100].

Figure 5-7 shows the schematic structure of a DSC. In this system, the temperatures of the sample and reference are controlled independently using separate, identical furnaces. The temperatures of the sample and reference are made identical by varying the power input to the two furnaces; The system monitors the temperature in both sample and reference. If the temperature differs from the programmed temperature, heat or coolant is supplied to that chamber to make the temperature equal the program temperature. A temperature difference between the sample and the reference is resulting from enthalpy or heat capacity changes in the sample. The temperature difference is recorded and related to enthalpy change in the sample by using calibration. About 10-20 mg sample is sealed into a small aluminium pan. The reference is usually an empty pan and cover. A flow of nitrogen gas is kept over the samples to create a reproducible and dry atmosphere.

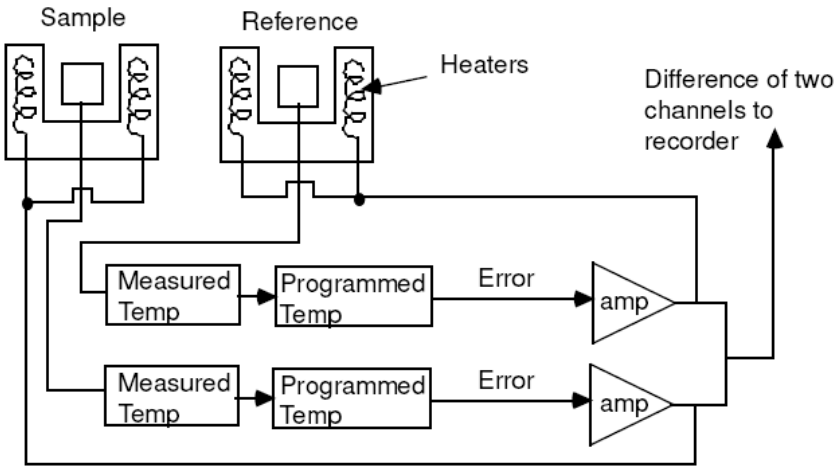

Figure 5-7 Schematic drawing of a DSC

A typical plot of heat flow with respect to temperature of wax crystallization process is given in Figure 5-8. During the cooling of a sample, waxes start to crystallize at onset temperature (T1) and two peaks are present; the end point is at T2. The baseline (the dot line) links the onset and end points.

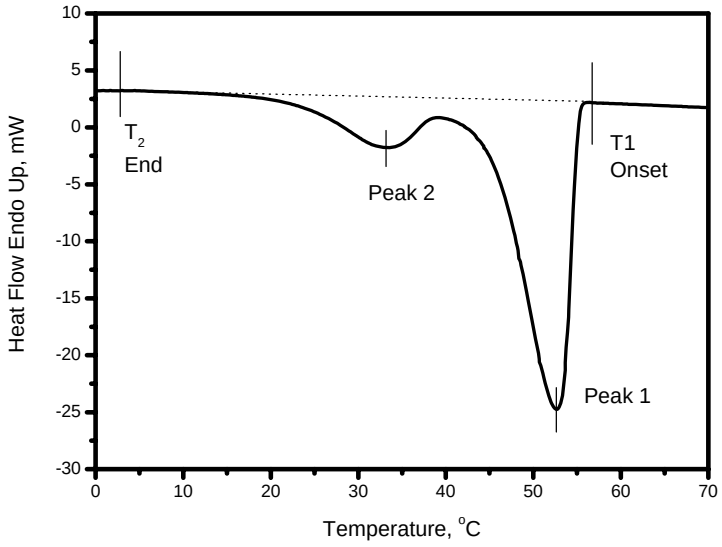

Figure 5-8 Typical DSC scan of wax crystallization process

Since the DSC is at constant pressure, heat flow is equivalent to enthalpy changes:

$$\left(\frac{dq}{dt}\right)_p = \frac{dH}{dt} \qquad (5\text{-}6)$$

Here dq/dt is the heat flow measured in mcal/sec. The heat flow difference between the sample and the reference is:

$$\Delta \frac{dH}{dt} = \left(\frac{dH}{dt}\right)_{sample} - \left(\frac{dH}{dt}\right)_{reference} \quad (5\text{-}7)$$

The integral under the DSC peak, above the baseline, gives the total enthalpy change for the process:

$$\int \left(\frac{dH}{dt}\right)_{sample} dt = \Delta H_{sample} \quad (5\text{-}8)$$

Combined with calibration constant and machine sensitivity coefficient, the heat per gram or enthalpy per gram of the transition is determined.

Heat capacities and changes in heat capacity can be determined from the shift in the baseline of the thermogram. The heat capacity is defined as:

$$C_p = \left(\frac{dq}{dT}\right)_p = \left(\frac{dH}{dT}\right)_p \quad (5\text{-}9)$$

5.5 Rheometry

Rheometry refers to the measuring techniques used to determine the rheological properties of materials. The most commonly used techniques can be grouped into three categories[101-103]:

---Capillary technique: in which the time for a fluid to flow through a capillary tube is measured.

---Falling/rolling ball technique, in which the time taken by a ball of known density rolling or falling through a certain distance in the test fluid is recorded.

---Rotational technique: in which rheometer determines the quantitative relationships between deformations and stresses.

Of which, rotational technique has been employed to widespread areas because of it's significant advantages in rapid response times, broad ranges of measuring geometries, and accurate velocity and temperature control in association with a computer.

Figure 5-9 [71] displays the scheme of rotational rheometer. It applies the stress via a motor and the strain is recorded. The viscosity and stress are calculated from torque and rotor speed measurements. The air bearing may give rise to greater sensitivity with low viscosity samples. Most rheometers are equipped with accurate thermostatic controls.

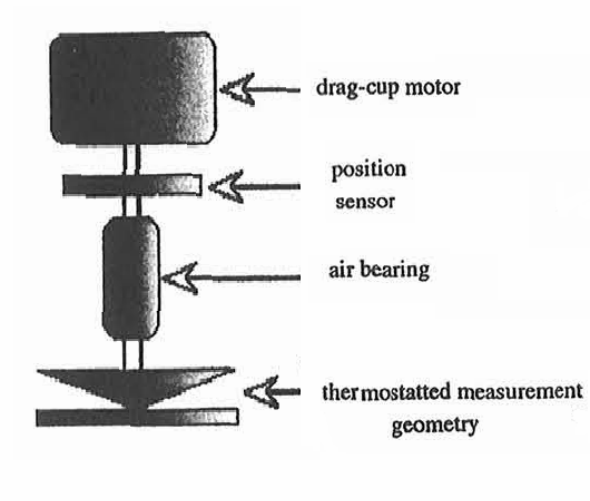

Figure 5-9 Schematic of rotational rheometer [71]

A range of different measuring geometries is available as accessory of rheometers, which can extend the measurement range. The most commonly employed geometries are shown in cross-section in Figure 5-10. There are two classical geometries in "cup and bob" viscometers, known as either the "Couette" or "Searle" systems - distinguished by whether the cup or bob rotates. The rotating cup is preferred in some cases, because it reduces the onset of Taylor vortices. Cone and Plate viscometers use a cone of very shallow angle in bare contact with a flat plate. The double gap rheometer is sensitive to low viscosity due to its larger contact area with samples. The parallel plate geometry has a wider measuring range, from viscosity lower than water to very high viscous samples.

Parallel-plate geometry was frequently used in this study of suspensions, emulsions and waxy oils. Generally. A significant feature of our MCR 301 rheometer is ‘‘True Gap’’ function which utilises a magnetic device to keep the gap distance constant during temperature scans. In this way fluctuations in gap distance, due to heat extension of the measuring system, were avoided. In addition, a heating cover was used to keep the temperature of the sample homogeneous at both the top and the bottom plate, and a solvent trap prevented evaporation from the sample.

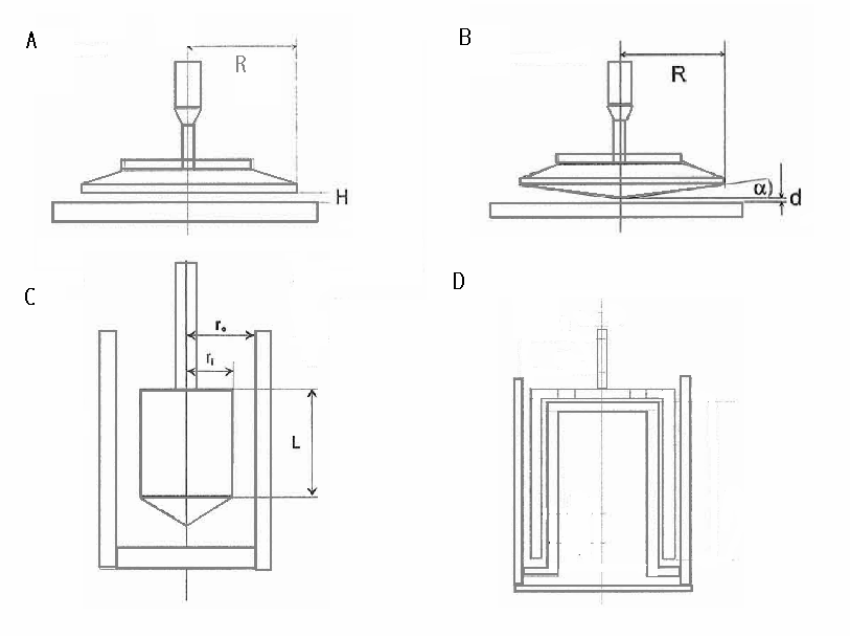

Figure 5-10 Cross-sections of common geometries:

A : Parallel plates, B: Cone and Plate, C: cup and bob, D: Double gap

6 Main Results

Paper 1 Rheological Properties of Aqueous Silica Particle Suspensions

The aim of this paper is to investigate the rheological properties of aqueous silica suspensions as a function of volume fraction of particles, particle size and shear rate. Monodisperse particles of 3 sizes (0.1, 0.5 and 1 μm) were synthesised according to the Stöber process. In addition 2 fumed silica samples (Aerosil 200 and Aerosil 380) were investigated.

The flow curves of the suspensions of all three silica particle sizes at 45 vol% are compared in Figure 6-1. The shear thinning effect becomes more pronounced as the particle size decreases, and this means that the viscosity differences are larger at low shear rates than at high shear rates. The higher viscosity at a given volume fraction for the smaller particle sizes is due to shorter interparticle distance and consequently the interactions between the particles are stronger compared to larger particles.

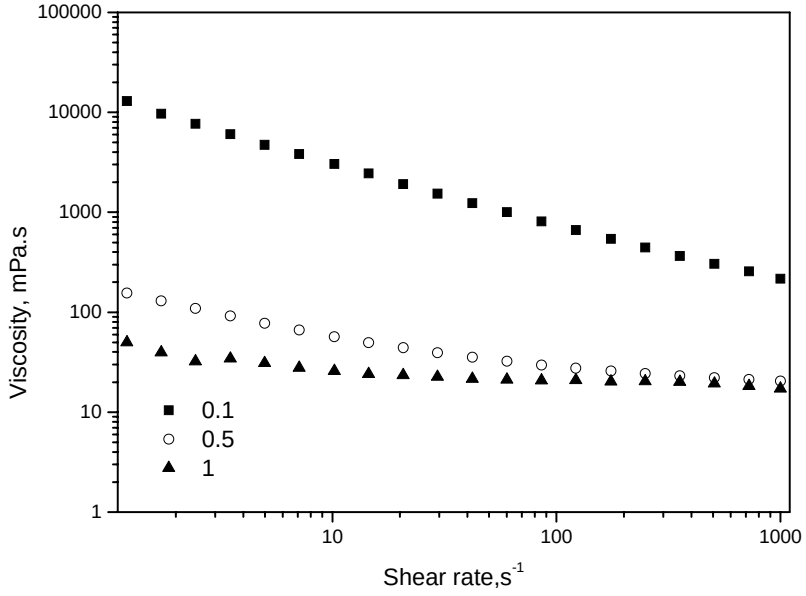

Figure 6-1: Flow curves for silica particle suspensions (0.1, 0.5 and 1 μm) at 45 vol% in 0.01M NaCl solution

The experimental data for the monodisperse silica particles were well fitted to the Mooney equation, Figure 6-2. The value of ϕ_m varies between 0.7 and 0.74, and this is close to the theoretical value of 0.74 for a close-packed array of same size spheres. The values of *a* are in the range 2.78- 4.90, similar to values estimated by Jeffrey [76]. The data in this study were

fitted to the Krieger and Dougherty equation as well, Figure 5. From the figure it is seen that both models fit very well for the 0.1µm particles, while the Krieger and Dougherty model gives the best fit for larger particles.

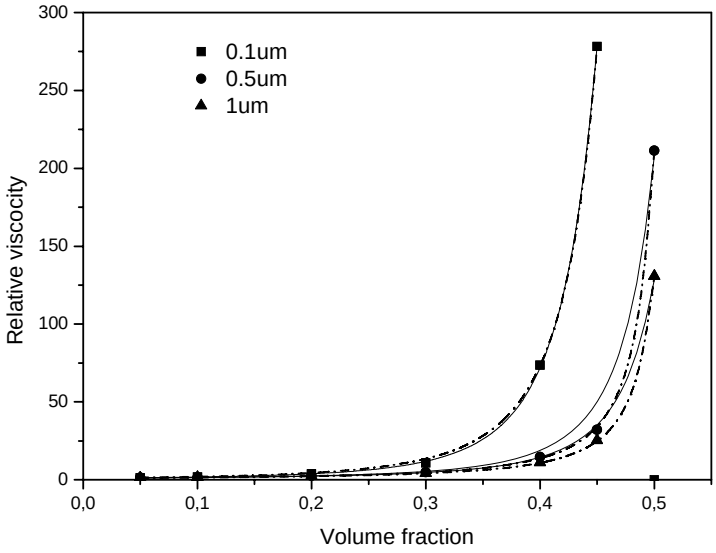

Figure 6-2: The relative viscosity (at shear rate 1000s $^{-1}$) for silica particles (0.1, 0.5 and 1 µm). The solid and dashed lines represent fit to the Mooney model and the Krieger and Dougherty model, respectively.

Synthesised silica Suspension had a Newtonian behaviour up to a particle volume fraction of 0.3. Oscillation measurements revealed that the suspensions exhibited elastic behaviour at higher particle fractions, and had liquid-like properties at lower volume fractions. Again Aerosil suspensions showed shear thinning behaviour at the highest volume fractions, and Newtonian behaviour at lower (<0.02) volume fractions.

Paper 2 Rheological Properties of Silica Particle Suspensions in Mineral Oil

In this paper we mainly focus on the rheological properties of particles suspended in a non-polar mineral oil as a function of volume fraction of particles, particle size, surface properties and shear rate. Three different types of particles were investigated: glass microspheres, monodisperse silica particles and fumed silica.

Figure 6-3 illustrates the flow curves of the all seven particle (glass microspheres and monodisperse silica particles) at 30 vol % in mineral oil. The three smaller monodisperse silica particle sizes display somewhat different degrees of shear thinning. The viscosities of the microspheres suspensions are independent of the shear rate in the higher shear rate range ($\geq 10s^{-1}$). In the lower shear rate range, however, there are some discrepancies between the samples. An explanation for this unusual behaviour can be that at low volume fractions, sedimentation effects are not negligible for these large particles.

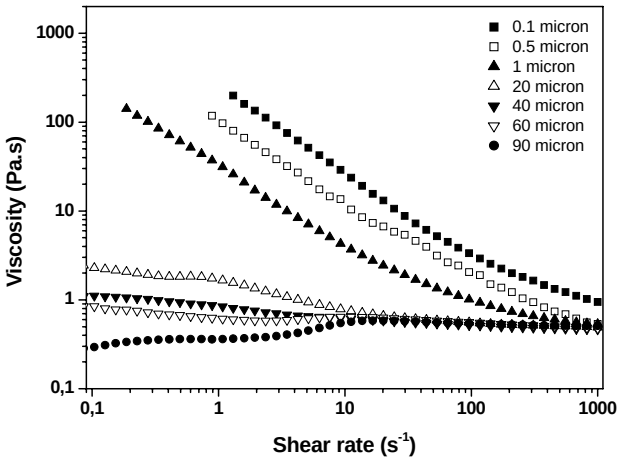

Figure 6-3: Flow curves for glass microspheres and silica particle suspensions at 30 vol%

Experimental data for the microspheres and monodisperse silica particles were fitted to the Krieger and Dougherty equation, Figure 6-4 and Figure 6-5, respectively. It is seen that the model fits quite well for both particle types, and consequently it can predict the relative viscosity at various volume fractions for a broad range of particle sizes. At a given shear rate, the maximum packing fraction, ϕ_m, and intrinsic viscosity, $[\eta]$, generally decrease as the particle size increases. As expected from the shear thinning behaviour, the value of $[\eta]$ is highest at lower shear rates. The value of ϕ_m varies between 0.59 and 0.80, which is close to the theoretical value of 0.74 for a close-packed array of same size spheres. The maximum

packing fraction mainly depends on the particle shape, size distribution and interaction force between the particles. For spherical particles, a broad size distribution can increase the value of the maximum packing fraction because smaller particles can fill the interspaces between larger particles. Strong repulsion may lead to a relatively open structure and a lower maximum packing fraction, whereas strong attraction between particles can form a tight packed array and increase the value. As the particle size decreases, the attraction force becomes more pronounced and maximum packing fractions accordingly increase. The maximum packing fraction also depends on the shear rate. Under low shear rate, the suspensions have a relatively compact structure and accordingly a higher maximum packing fraction. This microstructure is broken at higher shear rates.

For the Aerosil samples the values of maximum packing fraction were much lower, attributed to formation of branched aggregates. Nevertheless, the hydrophobic particles can be tighter packed than the hydrophilic particles. These interaction and packing considerations are also confirmed by the oscillation measurements.

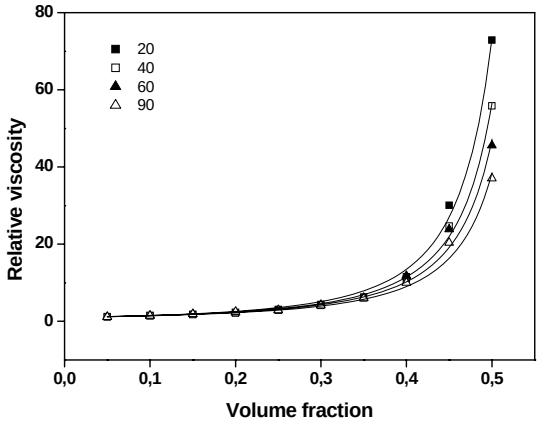

Figure 6-4: The relative viscosity (at shear rate 96s $^{-1}$)
for the microsphere silica. The line represents fit to the Krieger and Dougherty model

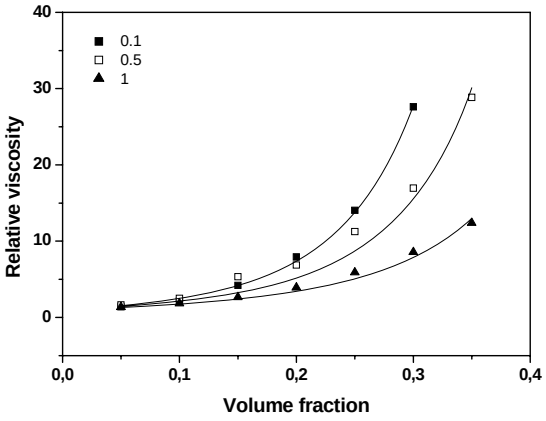

Figure 6-5: The relative viscosity (at shear rate 96s -1) for the synthesized silica particles. The line represents fit to the Krieger and Dougherty model

Paper 3 Effect of pH and salt on rheological properties of Aerosil suspensions

Ionic strength and pH influence the zeta potential of suspended particles, and consequently particle interactions and rheological properties as well. In this study the rheological properties and aggregation behaviour of Aerosil particles dispersed in aqueous solutions with various pH and salt concentration were studied. The relative viscosity as a function of volume fraction was fitted to the Krieger and Dougherty model for all the suspensions.

Figure 6-6 shows the Krieger and Dougherty equation fitted to the experimental data for suspensions at different pH. The model fits the data quite well and can be used to describe the relative viscosity over the entire pH range. The maximum packing fraction has a minimum at pH 4 (Isoelectric point) and reaches the highest values in the basic suspensions. The opposite is observed for the intrinsic viscosity. The maximum packing fraction is well correlated with interactions between the particles. Strong repulsion may lead to a relatively loose structure and a lower maximum packing fraction, whereas strong attraction between particles can form a tight packed array and increase the value. As the particle size decreases, the attraction force becomes more pronounced and maximum packing fractions accordingly increase.

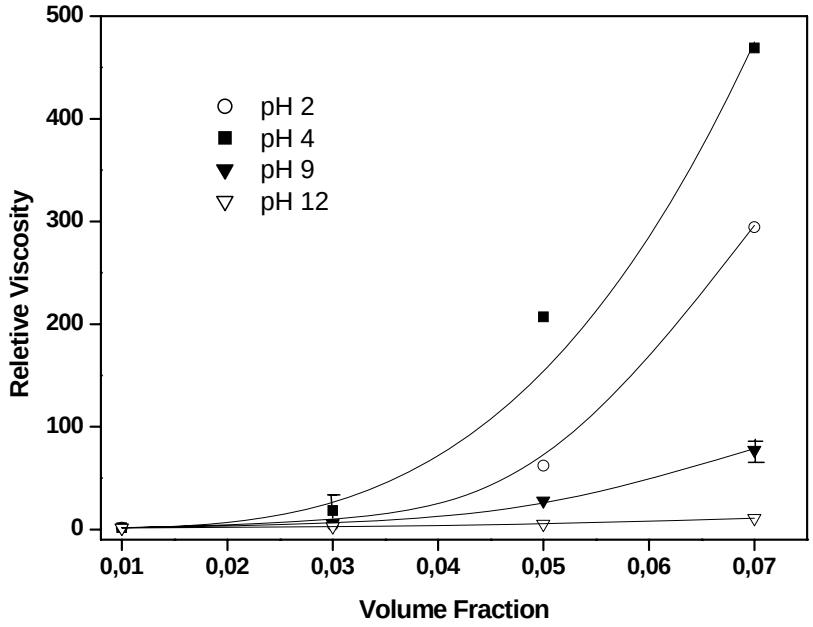

Figure 6-6: The relative viscosity (at shear rate 100s $^{-1}$) for Aerosil 200 suspended in 0.01M NaCl solution. The line represents the fit to the Krieger and Dougherty model.

The storage and the loss moduli at various frequencies for 0.01 M NaCl suspensions are shown in Figure 6-7. Below pH 7 both the storage and the loss moduli are constant over the

entire frequency range. The storage modulus is higher than the corresponding loss modulus, indicating that the suspensions display elastic behaviour. At pH 9 the storage modulus is slightly higher than the loss modulus up to 2 Hz, where there is a crossover point and the loss modulus becomes higher in value. This means that there is liquid-to-solid transition in the behaviour of the suspensions at this pH. At higher pH the viscous behaviour dominates in the suspensions as the loss modulus is higher than the storage modulus over the entire frequency range.

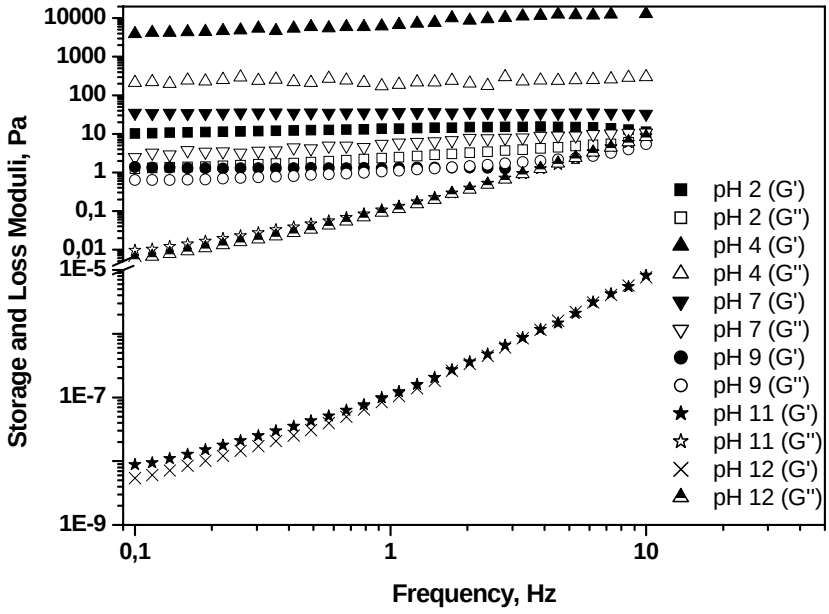

Figure 6-7: Storage and Loss moduli of suspensions at different pH (5% vol Aerosil 200)

Paper 4 Rheological Properties of Model and Crude Oil Systems when Wax Precipitate under Quiescent and Flowing Conditions

Wax precipitation and deposition is a recurring challenge in transportation of crude oil, and increased knowledge about the behaviour of such systems is necessary. Microscopy, rheometry and Differential Scanning Calorimetry (DSC) were used to follow the crystallisation of wax for two model systems. The amount of solid was also determined by the latter method as well. The flow and viscoelastic behaviour were investigated around the wax precipitation temperature, and the yield stress was determined both after dynamic and static cooling.

Long crystals were formed during low cooling rate, resulting in the strongest gel structures. The gels were formed at very low amounts of solid wax crystals (0.3-0.4 %), and wax precipitation was promoted by increased wax content dissolved in the samples. Dynamic cooling conditions decreased the gel strengths considerably as the imposed shear forces affect both crystal morphology and crystal-crystal interactions.

Figure 6-8 shows the viscosity as a function of temperature for wax A and B. The viscosity changes slowly with temperature above the WPT and the waxy systems behave as Newtonian liquids. The WPT for these measurements is defined as the temperature where the curves start to deviate from the Arrhenius equation, and a marked increase in the viscosity occurs as wax crystals start to precipitate. The values are slightly higher than those obtained during oscillation tests, but the trends are similar. The higher polydispersity of wax B is noticed by a more gradual evolution of the viscosity.

The difference between wax A and B is further underlined by looking at the viscosity at different amounts of precipitated wax, Figure 6-9. Wax A has steep increase in viscosity from 0.25 to 0.35 vol%, as wax precipitates and form a gel. Around 0.2 vol%, only a small inflection point is seen for wax B and the increase in viscosity is very small. Clearly, there are no strong interactions between the wax crystals in this case, and the network formation is not significant when the wax amount is less than 1 %.

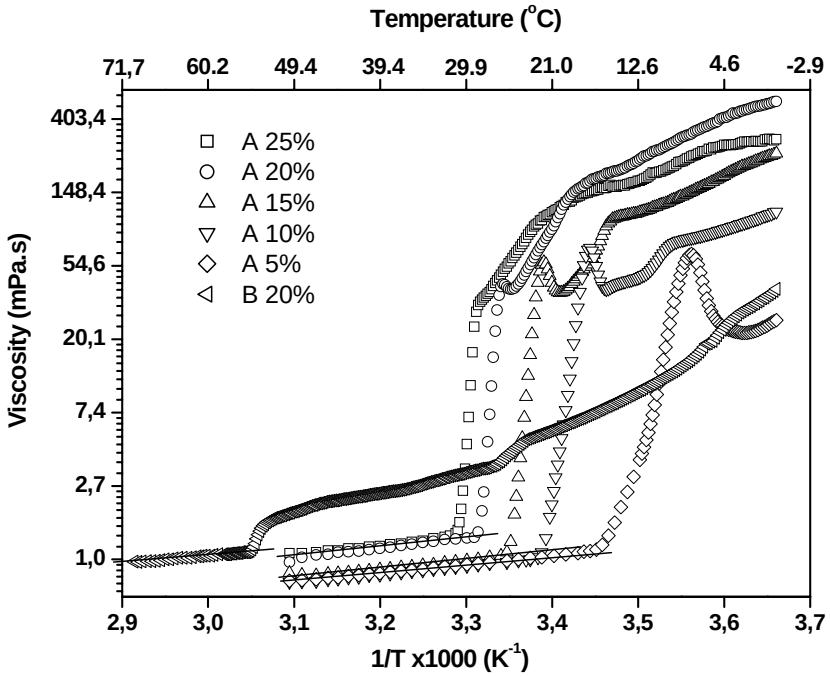

Figure 6-8: The temperature dependent behaviour of wax A and B during rotational conditions. The cooling rate was 2 ^{o}C/min and the shear rate kept constant at 100 s^{-1}.

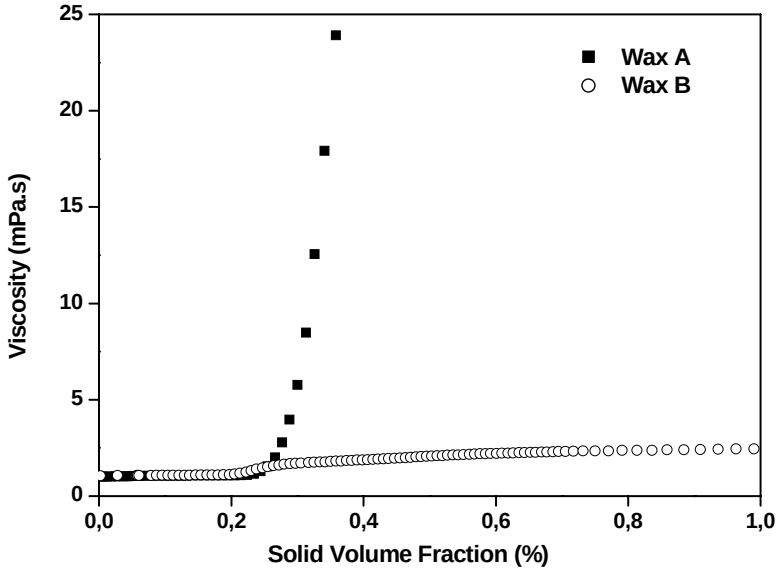

Figure 6-9: The viscosity of wax A and B (20% in decane) at low fractions of precipitated crystals

Two crude oils were investigated in order to evaluate their properties in view of the waxy model systems. The wax contents of the two oils were measured with DSC. For crude oil 1, its wax content is 3.1 % at 0^{o}C. Crude 2, on the other hand, contains very little wax (less than 0.2 % at 0^{o}C).

Temperature scans of the viscoelastic properties of the crude oils were determined (Figure 6-10). Clearly, the presence of wax influences the modules. Finite values of G'' confirms that both the crude oils behave as Newtonian fluids above the WPT. For Crude 1, the loss modulus start to increase around 31 ^{o}C, while crystal interactions is detected at 28 ^{o}C as the storage modulus appear. The storage modulus increases more rapidly than the loss modulus, and a gel point is found at 24 ^{o}C. For Crude 2, the elasticity modulus is very weak and noisy, and it has always lower values than the loss modulus. Consequently, the oil remains viscous even at low temperatures.

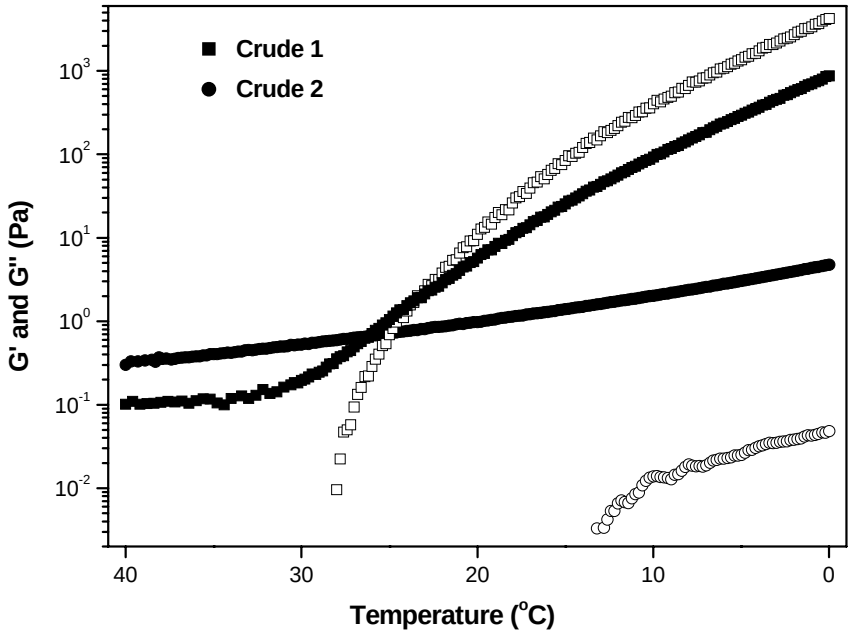

Figure 6-10: The temperature dependent behaviour of Crude 1 and Crude 2 determined under oscillating conditions and the cooling rate was 2 ^{o}C/min.
G' and G'' are shown by open and filled symbols, respectively.

Paper 5 Rheological Properties of Wax Containing Water-in-Oil Emulsions

Model emulsions with decane, toluene, asphathenes and paraffin in the continuous phase were prepared. Temperature scans of viscosity, flow measurements and yield stress measurements were carried out on the systems, and microscopy was used to determine water droplet size and appearance of wax crystals. The effects of water cut, asphaltene amount and wax amount were investigated, and the results interpreted in terms of microstructure and aggregate state of wax crystals and water droplets.

The yield stress was determined by subjecting the samples to an oscillating shear at a frequency of 0.1 Hz. Figure 6 displays the yield stress at 20^{o}C and 30^{o}C at various wax content in the continuous phase of the emulsions. Clearly, the yield stress is highest at 20 ^{o}C, where wax crystals have occurred in the system. As expected, the yield stress increases significantly with more wax in the oil phase.

Yield stress of nanoparticle suspensions was related to the volume fraction solid as follows :

$$\tau_y = k\phi^n \qquad (6\text{-}1)$$

where τ_y is the yield stress, k is a constant, ϕ is the solid volume fraction and n is a power index that indicate particle interactions. The equation fit these data quite well (dotted lines in Figure 6-11), and the power indexes are 9.6 and 5.9 at 20 and 30^{o}C, respectively. It follows that the highest interactions between wax crystals is at the lowest temperature.

The volume fraction of the dispersed phase is known to be a very important variable in emulsion rheology, and the relative viscosity of the suspension with respect to the pure fluid is often well described by the Krieger and Dougherty equation. Furthermore, the yield stress increases considerably as the water cut increases, Figure 6-12. The data fit nicely to equation 1 (dotted lines), and gives the following equation:

$$\tau_y = 3.2 \times \phi^{3.5}$$

Wax content and water cut has the most pronounced effect upon the viscosity and yield stress of the systems. The asphaltene content also result in increased viscosity and yield stress values, but to a lesser degree than the previous variables.

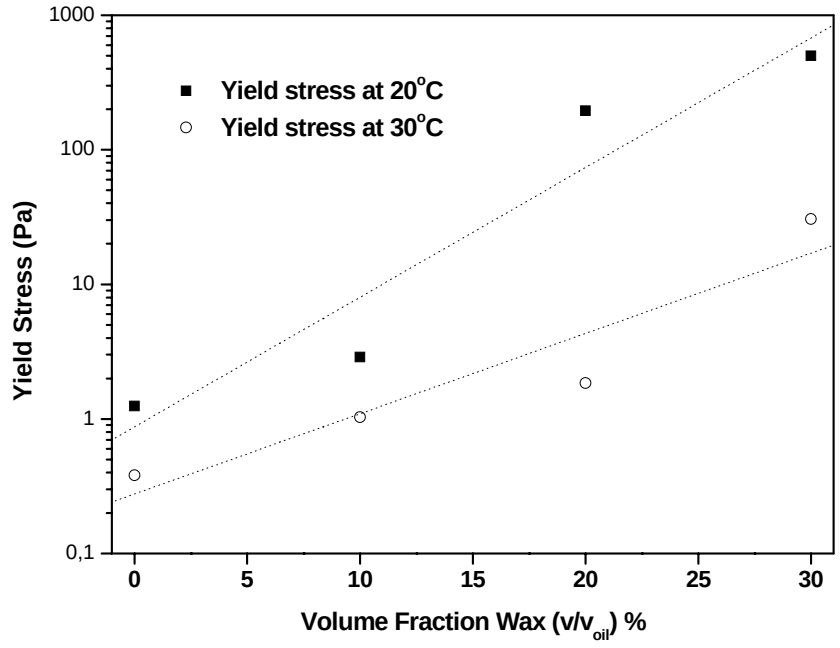

Figure 6-11: Yield stress at 20 °C and 30 °C for emulsions with different wax content. The dotted lines represent the fit to the power law equation.

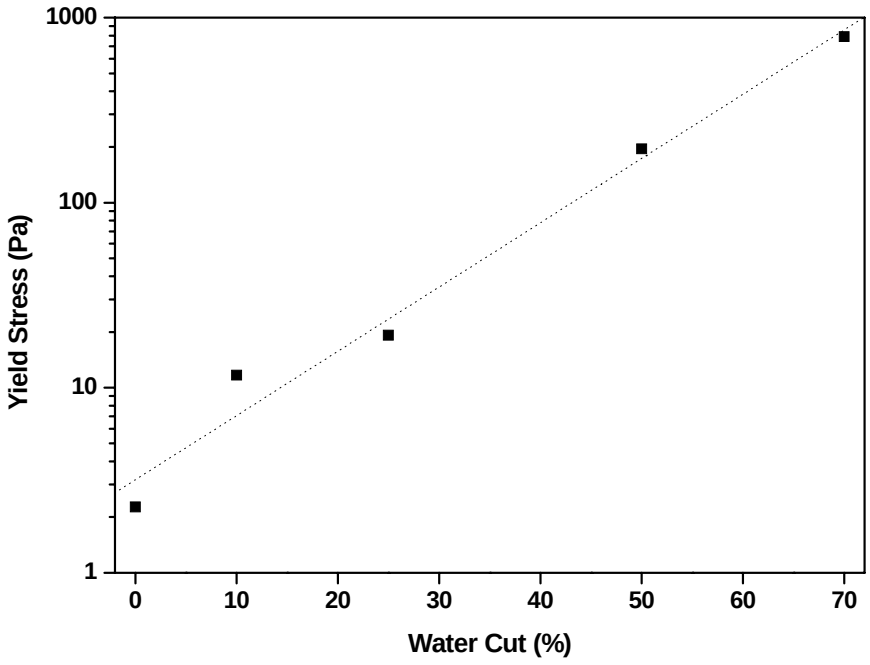

Figure 6-12 Yield stress at 20 °C for emulsions with different water cuts. The dotted line represent the fit to equation 6-1.

Concluding Remarks

The rheology of suspensions is a complex field that a range of variables influences. In this work, three different types of particles were investigated: glass microspheres, monodisperse silica particles and fumed silica. Mineral oil and aqueous solution acting as the continuous medium were studied as well.

The suspensions behaved Newtonian at dilute concentration. Shear thinning properties were observed at higher volume fractions. The shear thinning effect increased with decreasing particle size, due to stronger interparticle interactions between particles. Ionic strength and pH are both factors affect particle interactions and the rheological properties of suspensions. Large and strong aggregates were formed at the isoelectric point , due to the strong attraction between particles at this point. The larger aggregates results in higher viscosity, yield stress, storage moduli and shear thinning effects. The relative viscosity of all the suspensions can be reasonably well fitted to the Krieger and Dougherty model. The maximum packing fraction (ϕ_m) was close to the theoretical value for a close packed array (0.74) for the microspheres and synthesised particles. Furthermore, the value increased with decreasing particle size, again reflecting stronger attraction between the particles. For the Aerosil samples the values were much lower, attributed to formation of branched aggregates. Nevertheless, the hydrophobic particles can be tighter packed than the hydrophilic particles in mineral oil. These interaction and packing considerations are also confirmed by the oscillation measurements.

Wax precipitation and deposition is a recurring challenge in transportation of crude oil. The crystal growth of two model waxes has been investigated as a function of wax composition, cooling rate and cooling conditions (static or dynamic). Long crystals were formed during low cooling rate, resulting in the strongest gel structures. Dynamic cooling conditions decreased the gel strengths considerably as the imposed shear forces affect both crystal morphology and crystal-crystal interactions. The transition into gel structures occur in a narrow temperature interval for the model wax with the smallest distribution, while more gradual transition was found for the polydisperse model wax.

The rheological properties of emulsions containing wax stabilized by asphaltenes were studied. Wax content and water cut has the most pronounced effect upon the viscosity and yield stress of the systems. The asphaltene content also result in increased viscosity and yield stress values, but to a lesser degree than the previous variables.

References

1. Kelland, M.A., *History of the Development of Low Dosage Hydrate Inhibitors.* Energy & Fuels, 2006. **20**(3): p. 825-847.
2. Guo, T.-M., et al., *A review on the gas hydrate research in China.* Journal of Petroleum Science & Engineering, 2004. **41**(1-3): p. 11-20.
3. Venkatesan, R., et al., *The strength of paraffin gels formed under static and flow conditions.* Chemical Engineering Science, 2005. **60**(13): p. 3587-3598.
4. Dabir, B., et al., *Asphalt flocculation and deposition. III. The molecular weight distribution.* Fuel, 1996. **75**(14): p. 1633-1645.
5. Sjöblom, J., et al., *Our current understanding of water-in-crude oil emulsions. Recent characterization techniques and high pressure performance.* Advances in Colloid and Interface Science, 2003. **100-102**: p. 399-473.
6. Johnsen, E.E. and H.P. Rønningsen, *Viscosity of 'live' water-in-crude-oil emulsions: experimental work and validation of correlations.* Journal of Petroleum Science & Engineering, 2003. **38**(1-2): p. 23-36.
7. Hiemenz, P.C., R. Rajagopalan, and Editors, *Principles of Colloid and Surface Chemistry, Third Edition, Revised and Expanded*. 1997. 688 pp.
8. Schramm, L.L., *Suspensions: basic principles.* Advances in Chemistry Series, 1996. **251**(Suspensions: Fundamentals and Applications in the Petroleum Industry): p. 3-44.
9. Adachi, N., M. Hashiba, and O. Sakurada, *Rheological properties of slurries prepared using a planetary mixer.* Ceramics International, 2004. **30**(6): p. 1055-1058.
10. Hassan, M.S. and N.A. Abdel-Khalek, *Beneficiation and applications of an Egyptian bentonite.* Applied Clay Science, 1998. **13**(2): p. 99-115.
11. Strivens, T.A., *The Rheology of Paints*, in *Paint and Surface Coatings--Theory and Practice*, R. Lambourne and T.A. Strivens, Editors. 1999, Woodhead Publishing Ltd: Cambrige, England. p. 575-597.
12. Tsutsumi, A. and K. Yoshida, *Rheological behavior of coal-solvent slurries.* Fuel, 1986. **65**(7): p. 906-9.
13. Flatt, R.J. and P. Bowen, *Electrostatic repulsion between particles in cement suspensions: Domain of validity of linearized Poisson-Boltzmann equation for nonideal electrolytes.* Cement and Concrete Research, 2003. **33**(6): p. 781-791.
14. Tadros, T.F., *Correlation of viscoelastic properties of stable and flocculated suspensions with their interparticle interactions.* Advances in Colloid and Interface Science, 1996. **68**: p. 97-200.
15. Holmberg, K., et al., *Surfactants and Polymers in Aqueous Solution*. 2nd Edition ed. 2002, Chichester, UK: Wiley. 175-191.
16. Barnes, H.A., J.F. Hutton, and K. Walters, *An introduction to rheology*. 1989, Amsterdam, the Netherlands: Elsevier Sci. 115-140.
17. Morrison, I.D. and S. Ross, *Colloidal Dispersions: Suspensions, Emulsions, and Foams*. 2002.
18. Barthel, H., et al., *Fumed silica - rheological additive for adhesives, resins, and paints.* Macromolecular Symposia, 2002. **187**: p. 573-584.
19. Shaw, D.J., *Introduction to Colloid and Surface Chemistry. 4th Ed*. 1991. 306.
20. Derjaguin, B.V. and L. Landau, *Theory of the Stability of Strongly Charged Lyophobic Sols and of the Adhesion of Strongly Charged Particles in Solutions of Electrolytes.* Acta Physicochimica URSS, 1941. **14**: p. 663-662.

21. Verwey, E.J.W. and J.T.G. Overbeek, *Theory of the Stability of Lyophobic Colloids.* 1948. 216 pp.
22. Yoon, R.-H. and S. Vivek, *Effects of short-chain alcohols and pyridine on the hydration forces between silica surfaces.* Journal of Colloid and Interface Science, 1998. **204**(1): p. 179-186.
23. Horn, R.G., D.T. Smith, and W. Haller, *Surface forces and viscosity of water measured between silica sheets.* Chemical Physics Letters, 1989. **162**(4-5): p. 404-8.
24. Grabbe, A. and R.G. Horn, *Double-layer and hydration forces measured between silica sheets subjected to various surface treatments.* Journal of Colloid and Interface Science, 1993. **157**(2): p. 375-83.
25. Chapel, J.P., *Electrolyte Species Dependent Hydration Forces between Silica Surfaces.* Langmuir, 1994. **10**(11): p. 4237-43.
26. Yotsumoto, H. and R.H. Yoon, *Application of extended DLVO Theory. I. Stability of rutile suspensions.* Journal of Colloid and Interface Science, 1993. **157**(2): p. 426-33.
27. Yoon, R.-H. and S.A. Ravishankar, *Application of extended DLVO theory III. Effect of octanol on the long-range hydrophobic forces between dodecylamine-coated mica surfaces.* Journal of Colloid and Interface Science, 1994. **166**(1): p. 215-24.
28. Yotsumoto, H. and R.H. Yoon, *Application of extended DLVO theory. II. Stability of silica suspensions.* Journal of Colloid and Interface Science, 1993. **157**(2): p. 434-41.
29. Savarmand, S., et al., *Rheological properties of concentrated aqueous silica suspensions. Effects of pH and ions content.* Journal of Rheology 2003. **47**(5): p. 1133-1149.
30. Zaman, A.A., et al., *Rheological behavior of highly concentrated aqueous silica suspensions in the presence of sodium nitrate and polyethylene oxide.* Journal of Rheology 1996. **40**(6): p. 1191-1210.
31. Hiemenz, P.C., *Principles of Colloid and Surface Chemistry, 2nd Edition*. 1986. 188.
32. Speight, J.G., *The Chemistry and Technology of Petroleum, Third Edition, Revised and Expanded. [In: Chem. Ind. (Dekker), 1998; 76]*. 1998. 918 pp.
33. Speight, J.G., *The chemical and physical structure of petroleum: effects on recovery operations.* Journal of Petroleum Science and Engineering, 1999. **22**(1-3): p. 3-15.
34. Speight, J.G. and Editor, *Petroleum Chemistry and Refining*. 1998. 273 pp.
35. Rønningsen, H.P.B., Brit., *Wax Precipitation from North Sea Crude Oils. 1. Crystallization and Dissolution Temperatures, and Newtonian and Non-Newtonian Flow Properties.* Energy & Fuels 1991. **5**: p. 895-908.
36. Wardhaugh, L.T. and D.V. Boger, *Flow characteristics of waxy crude oils: application to pipeline design.* AIChE Journal, 1991. **37**(6): p. 871-85.
37. Wardhaugh, L.T.B., D.V., *The measurement and description of the yielding behavior of waxy crude oil.* J. Rheol., 1991. **35**: p. 1121-1156.
38. Sjöblom, J., et al., *Demulsifiers in the oil industry*, in *Encyclopedic hanbook of emulsion technology* J. Sjöblom, Editor. 2001, Marcel Dekker, Inc.: Newyork. p. 595-619.
39. Ali, M.A. and W.A. Nofal, *Application of high performance liquid chromatography for hydrocarbon group type analysis of crude oils.* Fuel Science & Technology International, 1994. **12**(1): p. 21-33.
40. Sjöblom, J., et al., *Our current understanding of water-in-crude oil emulsions.: Recent characterization techniques and high pressure performance.* Advances in Colloid and Interface Science, 2003. **100-102**: p. 399-473.
41. Radke, M., H. Willsch, and D.H. Welte, *Preparative hydrocarbon group type determination by automated medium pressure liquid chromatography.* Analytical Chemistry, 1980. **52**(3): p. 406-11.

42. Suatoni, J.C. and R.E. Swab, *Rapid hydrocarbon group-type analysis by high performance liquid chromatography.* Journal of Chromatographic Science, 1975. **13**(8): p. 361-6.
43. Lundanes, E. and T. Greibrokk, *Separation of fuels, heavy fractions, and crude oils into compound classes: a review.* Journal of High Resolution Chromatography, 1994. **17**(4): p. 197-202.
44. Aske, N., H. Kallevik, and J. Sjoeblom, *Determination of Saturate, Aromatic, Resin, and Asphaltenic (SARA) Components in Crude Oils by Means of Infrared and Near-Infrared Spectroscopy.* Energy & Fuels, 2001. **15**(5): p. 1304-1312.
45. Andersen, S.I. and K.S. Birdi, *Influence of temperature and solvent on the precipitation of asphaltenes.* Fuel Science & Technology International, 1990. **8**(6): p. 593-615.
46. Speight, J.G. and R.b. Long, *The concept of asphaltenes revisited.* Fuel Science & Technology International, 1996. **14**(1 & 2): p. 1-12.
47. Havre, T.E., *Formation of Calcium Naphthenate in Water/Oil Systems, Naphthenic Acid Chemistry and Emulsion Stability*. 2002, Department of Chemical Engineering, Norwegian University of Science and Technology: Trondheim.
48. Kallevik, H., *Characterisation of Crude Oil and Model Oil Emulsions by means of Near Infrared Spectroscopy and Multivariate Analysis*. 1999, Department of Chemistry, University of Bergen: Bergen.
49. Groenzin, H. and O.C. Mullins, *Molecular Size and Structure of Asphaltenes from Various Sources.* Energy & Fuels, 2000. **14**(3): p. 677-684.
50. Groenzin, H. and O.C. Mullins, *Asphaltene molecular size and structure.* Journal of Physical Chemistry A, 1999. **103**(50): p. 11237-11245.
51. Holmberg, K., et al., *Surfactants and Polymers in Aqueous Solution, 2nd Edition.* 2002. 544 pp.
52. Hunter, R.J., *Introduction to Modern Colloid Science*. 1993. 338 pp.
53. Li, M., et al., *Studies on properties of interfacial active fractions from crude and their effect on stability of crude emulsions.* Journal of Dispersion Science and Technology, 2006. **27**(5): p. 677-687.
54. Hemmingsen, P.V., et al., *Emulsions of heavy crude oils. I: Influence of viscosity, temperature, and dilution.* Journal of Dispersion Science and Technology, 2005. **26**(5): p. 615-627.
55. Sullivan, A.P. and P.K. Kilpatrick, *The Effects of Inorganic Solid Particles on Water and Crude Oil Emulsion Stability.* Industrial & Engineering Chemistry Research, 2002. **41**(14): p. 3389-3404.
56. Ali, M.F. and M.H. Alqam, *The role of asphaltenes, resins and other solids in the stabilization of water in oil emulsions and its effects on oil production in Saudi oil fields.* Fuel, 2000. **79**(11): p. 1309-1316.
57. Li, M., et al., *A study on stability of water-in-crude oil emulsions. VI. Influence of wax particles on properties of interfacial film between oil and water.* Shiyou Xuebao, Shiyou Jiagong, 1999. **15**(5): p. 1-5.
58. Sjöblom, J., et al., *Water-in-crude-oil emulsions from the Norwegian continental shelf. 7. Interfacial pressure and emulsion stability.* Colloids and Surfaces, 1992. **66**(1): p. 55-62.
59. Sjöblom, J., et al., *Water-in-crude oil emulsions from the Norwegian continental shelf. 10. Aging of the interfacially active components and the influence on the emulsion stability.* Colloids and Surfaces, A: Physicochemical and Engineering Aspects, 1995. **96**(3): p. 261-72.

60. Spiecker, P.M., K.L. Gawrys, and P.K. Kilpatrick, *Aggregation and solubility behavior of asphaltenes and their subfractions.* Journal of Colloid and Interface Science, 2003. **267**(1): p. 178-193.
61. Spiecker, P.M., et al., *Effects of petroleum resins on asphaltene aggregation and water-in-oil emulsion formation.* Colloids and Surfaces, A: Physicochemical and Engineering Aspects, 2003. **220**(1-3): p. 9-27.
62. Djuve, J., et al., *Chemical destabilization of crude oil based emulsions and asphaltene stabilized emulsions.* Colloid and Polymer Science, 2001. **279**(3): p. 232-239.
63. McLean, J.D. and P.K. Kilpatrick, *Effects of asphaltene aggregation in model heptane-toluene mixtures on stability of water-in-oil emulsions.* Journal of Colloid and Interface Science, 1997. **196**(1): p. 23-34.
64. McLean, J.D. and P.K. Kilpatrick, *Effects of asphaltene solvency on stability of water-in-crude-oil emulsions.* Journal of Colloid and Interface Science, 1997. **189**(2): p. 242-253.
65. Bott, T.R. and J.S. Gudmundsson, *Deposition of paraffin from kerosene in cooled heat exchanger tubes.* Canadian Journal of Chemical Engineering, 1977. **55**(4): p. 381-5.
66. Agrawal, K.M., et al., *Wax deposition of Bombay high crude oil under flowing conditions.* Fuel, 1990. **69**(6): p. 794-6.
67. Visintin, R.F.G., et al., *Rheological Behavior and Structural Interpretation of Waxy Crude Oil Gels.* Langmuir, 2005. **21**(14): p. 6240-6249.
68. Kane, M., et al., *Morphology of paraffin crystals in waxy crude oils cooled in quiescent conditions and under flow.* Fuel, 2002. **82**(2): p. 127-135.
69. Dirand, M., et al., *Multicomponent paraffin waxes and petroleum solid deposits: structural and thermodynamic state.* Fuel, 1998. **77**(12): p. 1253-1260.
70. Chen, S., G. Øye, and J. Sjöblom, *Rheological Properties of Model and Crude Oil Systems when Wax Precipitate under Quiescent and Flowing Conditions* Journal of Dispersion Science and Technology, 2007. **28**(6).
71. Goodwin, J. and R.W. Hughes, *Rheology for Chemists: An Introduction*. 2000. 250 pp.
72. Goodwin, J.W.H., R.W., *Rheology for chemists- an introduction*. 2000, Cambridge, UK: The royal Society of Chemistry. 102-4.
73. Steffe, J.F., *Rheological methods in food process enginnering* 1996. 428.
74. Krieger, I.M. and T.J. Dougherty, *A mechanism for non-Newtonian flow in suspensions of rigid spheres.* Transactions of the Society of Rheology, 1959. **3**: p. 137-52.
75. Mooney, M., *The viscosity of a concentrated suspension of spherical particles.* Journal of Colloid Science, 1951. **6**: p. 162-70.
76. Jeffrey, D.J. and A. Acrivos, *The rheological properties of suspensions of rigid particles.* AIChE Journal, 1976. **22**(3): p. 417-32.
77. Van der Werff, J.C. and C.G. De Kruif, *Hard-sphere colloidal dispersions: the scaling of rheological properties with particle size, volume fraction, and shear rate.* Journal of Rheology (New York, NY, United States), 1989. **33**(3): p. 421-54.
78. Olhero, S.M. and J.M.F. Ferreira, *Influence of particle size distribution on rheology and particle packing of silica-based suspensions.* Powder Technology, 2004. **139**(1): p. 69-75.
79. Lee, J.-D., J.-H. So, and S.-M. Yang, *Rheological behavior and stability of concentrated silica suspensions.* Journal of Rheology (New York), 1999. **43**(5): p. 1117-1140.

80. Zaman, A.A., et al., *Rheological behavior of highly concentrated aqueous silica suspensions in the presence of sodium nitrate and polyethylene oxide.* Journal of Rheology (New York), 1996. **40**(6): p. 1191-1210.
81. Zaman, A.A. and B.M. Moudgil, *Rheology of bidisperse aqueous silica suspensions: A new scaling method for the bidisperse viscosity.* Journal of Rheology (New York), 1998. **42**(1): p. 21-39.
82. Mewis, J., *Flow behavior of concentrated suspensions: predictions and measurements.* International Journal of Mineral Processing, 1996. **44-45**: p. 17-27.
83. Chong, J.S., E.B. Christiansen, and A.D. Baer, *Rheology of concentrated suspensions.* Journal of Applied Polymer Science, 1971. **15**(8): p. 2007-21.
84. Metzner, A.B., *Rheology of suspensions in polymeric liquids.* Journal of Rheology (New York, NY, United States), 1985. **29**(6): p. 739-75.
85. Giesekus, H., *Stressing behavior in simple shear flow as predicted by a new constitutive model for polymer fluids.* Journal of Non-Newtonian Fluid Mechanics, 1983. **12**(3): p. 367-74.
86. Watanabe, T., M. Aoshima, and A. Satoh, *Rheological properties and particle behaviors of a nondilute colloidal dispersion composed of ferromagnetic spherocylinder particles subjected to a simple shear flow: Analysis by means of mean-field approximation for the two typical external magnetic field directions.* Journal of Colloid and Interface Science, 2006. **302**(1): p. 347-355.
87. Asokan, K., et al., *Review of chaos in the dynamics and rheology of suspensions of orientable particles in simple shear flow subject to an external periodic force.* Journal of Non-Newtonian Fluid Mechanics, 2005. **129**(3): p. 128-142.
88. Asokan, K. and T.R. Ramamohan, *The rheology of a dilute suspension of Brownian dipolar spheroids in a simple shear flow under the action of an external force.* Physics of Fluids, 2004. **16**(2): p. 433-444.
89. Manhart, M., *Rheology of suspensions of rigid-rod like particles in turbulent channel flow.* Journal of Non-Newtonian Fluid Mechanics, 2003. **112**(2-3): p. 269-293.
90. Fuchs, M. and M.E. Cates, *Non-Newtonian viscosity of interacting Brownian particles: comparison of theory and data.* Los Alamos National Laboratory, Preprint Archive, Condensed Matter, 2002: p. 1-6, arXiv:cond-mat/0210194.
91. Bergenholtz, J., J.F. Brady, and M. Vicic, *The non-Newtonian rheology of dilute colloidal suspensions.* Journal of Fluid Mechanics, 2002. **456**: p. 239-275.
92. Foss, D.R. and J.F. Brady, *Structure, diffusion and rheology of Brownian suspensions by Stokesian dynamics simulation.* Journal of Fluid Mechanics, 2000. **407**: p. 167-200.
93. Wierenga, A.M. and A.P. Philipse, *Low-shear viscosity of isotropic dispersions of (Brownian) rods and fibers; a review of theory and experiments.* Colloids and Surfaces, A: Physicochemical and Engineering Aspects, 1998. **137**(1-3): p. 355-372.
94. Exl, F. and J. Kindersberger. *Contact Angle Measurement on Insulator Surfaces with Artificial Pollution Layers and Various Surface Roughnesses*. in *Proceedings of the XIVth International Symposium on High Voltage Engineering,*. 2005.
95. Sjoeblom, J., et al., *Modern characterization techniques for crude oils, their emulsions, and functionalized surfaces.* Surfactant Science Series, 2006. **132**(Emulsions and Emulsion Stability (2nd Edition)): p. 415-476.
96. Henry, D.C., *The cataphoresis of suspended particles. I. The equation of cataphoresis.* Proc.Roy.Soc., 1931. **106**(A133): p. 106-29.
97. Stank, J. and J. Mullay, *Analysis of wax-oil mixtures using differential scanning calorimetry (DSC).* Thermochimica Acta, 1986. **105**: p. 9-17.

98. Kok, M.V., et al., *Comparison of wax appearance temperatures of crude oils by differential scanning calorimetry, thermo-microscopy and viscometry.* Fuel, 1996. **75**(7): p. 787-790.
99. Y.P. Claudy, J.M.L., C. Benoit, O. Jean,, Fuel., 1988. **66**(1): p. 58-61.
100. Letoffe, J.M., et al., *Crude oils: characterization of waxes precipitated on cooling by d.s.c. and thermomicroscopy.* Fuel, 1995. **74**(6): p. 810-17.
101. Carter, R.E., *Capillary extrusion rheometry in ceramics-processing technology.* American Ceramic Society Bulletin, 2001. **80**(6): p. 23-26.
102. Barnes, H.A. and Q.D. Nguyen, *Rotating vane rheometry - a review.* Journal of Non-Newtonian Fluid Mechanics, 2001. **98**(1): p. 1-14.
103. Reinhardt, U., *Rotational rheometry. A look into the future.* Applied Rheology, 1997. **7**(1): p. 25-31.